OUTPUT FREQUENCY CHANGES IN A COMMERCIAL RUBIDIUM CLOCK RESULTING FROM MAGNETIC FIELD AND MICROWAVE POWER VARIATIONS

THESIS

Edward B. Sarosy, Major, USAF

AFIT/GE/ENG/92S-01

DEPARTMENT OF THE AIR FORCE
AIR UNIVERSITY
AIR FORCE INSTITUTE OF TECHNOLOGY

Wright-Patterson Air Force Base, Ohio

AFIT/GE/ENG/92S-01

OUTPUT FREQUENCY CHANGES IN A COMMERCIAL RUBIDIUM CLOCK RESULTING FROM MAGNETIC FIELD AND MICROWAVE POWER VARIATIONS

THESIS

Edward B. Sarosy, Major, USAF

AFIT/GE/ENG/92S-01

Approved for Public Release; Distribution Unlimited

AFIT/GE/ENG/92S-01

OUTPUT FREQUENCY CHANGES IN A COMMERCIAL RUBIDIUM CLOCK RESULTING FROM MAGNETIC FIELD AND MICROWAVE POWER VARIATIONS

THESIS

Presented to the Faculty of the School of Engineering

of the Air Force Institute of Technology

Air University

In Partial Fulfillment of the

Requirements for the Degree of

Master of Science in Electrical Engineering

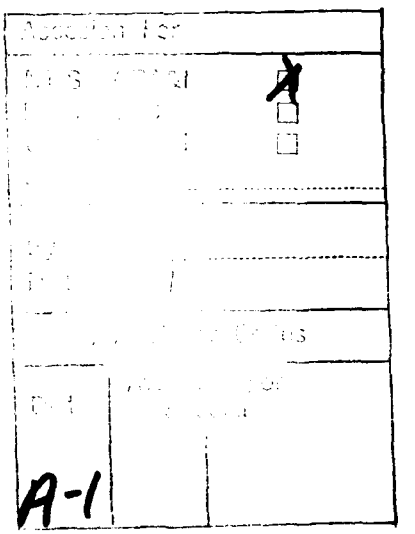

Edward B. Sarosy, B.S.

Major, USAF

September 1992

Approved for Public Release; Distribution Unlimited

Acknowledgements

In performing the experimentation and writing this thesis I have had a great deal of help from others. I appreciate the suggestion from Col. Lawrence Graviss in the selection of this thesis topic, and the support he has given me in completing the experiments and analysis.

I would like to extend my appreciation to Dr. Riley of EG&G Frequency Products for his support and cooperation in conducting this experiment. His timely responses to my many questions allowed for the successful completion of this study.

I would also like to thank Mr Charles Karuza, Mr Walter Johnson and Mr Frank Voit of the Engineering Lab at Los Angeles AFB, California for their assistance, patience and cooperation during the experimental stages of the thesis. I would like to thank my thesis adviser Capt Philip Joseph for his time and help in completing my masters degree requirements. Finally, I would like to give special thanks and appreciation to my wife Jeani for her support, help and understanding during two thesis projects.

Edward B. Sarosy

Table of Contents

List of Figures

List of Tables

Abstract

The objective of this experiment was to show the relationship between output frequency shifts and the absorption cell magnetic field during microwave power fluctuations on a commercial (EG&G Frequency Products; Model RFS-10) rubidium frequency clock. This experiment was conducted at the Aerospace Corp. frequency laboratory in El Segundo, Ca.

Changes in the clock output frequency relative to the 10 MHz reference were monitored as changes in the absorption cell magnetic field (0.01 to 1.0 Gauss) and changes in the cell's interrogation microwave power were varied from the nominal factory specification (P_0) at four discrete values (+1.3, -1.1, -2.2, -4.0 dB). The data presented here represents the difference between two 1000-second frequency averages, calculated as the difference in output frequency at the average high power (f_H) and that at the average low power (f_L) and normalized to the nominal output (i.e. $(f_H - f_L)/10$ MHz). The maximum normalized output frequency shift of 1.4×10^{-10} occurred at -4dB. The maximum normalized frequency change for the +1.3 and -1.1 dB data is about 3×10^{-11} and for the -2.2 dB data is about 6×10^{-11}. As a function of the change in microwave power, the maximum frequency change is about 2.6×10^{-11} per dB of power change. There also existed several magnetic field values which resulted in minimum output frequency change. This occurred at absorption cell magnetic field values of 9 and 27 milli-Gauss, where the nominal setting is 137 milli-Gauss.

A minor design change in the electronics package is recommended to control input microwave power to within 0.01 dB. Use of low cell magnetic field values to control frequency shifts cannot be made at this time until a larger sample of clocks are tested.

I. *Introduction*

Atomic frequency standards are very stable and accurate frequency sources. Space applications rely heavily on accurate clocks for navigation and communication applications, which in turn are based on frequency standards. (20:537-539)

This section provides an introduction to the components of atomic standards, to the measurement approaches used, and a brief description of what makes atomic standards operate. Also, a description of the operating characteristics of the specific rubidium frequency standard used in this experiment will be provided. At the conclusion of this section there will be a discussion of why the test results are of importance and what impact they could have on future rubidium clock design and operation.

Frequency is a quantity closely related to time, sometimes referred to as its inverse. In actuality, frequency is derived from the observations of periodic events, which occur at regular intervals (of time). If constant, this interval is called the period (T) and the frequency of the oscillation (υ), measured in Hertz, is the inverse of the period:

$$\upsilon = 1/T \qquad 1\text{-}1$$

One hertz is one period (or cycle) per second. An outstanding feature of frequency and time is the high accuracy of this basic definition and precision of the measurements, which during the last twenty-five years have progressed to extremely precise levels. (18:2)

The basic unit of time is the second (s). Since 1967, one second is defined as "the duration of 9,192,631,770 periods of the radiation corresponding to the transition between the two hyperfine levels of the ground state of the Cesium-133 atom" (14:4), where the accuracy of this period is good through the tenth significant digit. Therefore, the frequency of the Cesium oscillations are 9.192631770 GHz. Because of this type of accuracy, cesium clocks have been widely used as standards for precise time, as well as used for test equipment, to evaluate new types of frequency standards. If cesium is so accurate, then why are other types of standards being investigated? Compared to rubidium clocks, cesium is on the average 15 times larger, 10 times heavier and requires twice the power. However, cesium still out performs rubidium in terms of long-term accuracy by more than an order of magnitude. Because of these reasons, and the need to conserve space and power for satellite operations, increased research into improved rubidium clock accuracy has been accomplished over the past several years.

Accuracy, Reproducibility, Stability

The performance of frequency standards and clocks is described in terms of accuracy, reproducibility and stability. Accuracy is the degree of conformity of a measured and/or calculated value to a specified value. Reproducibility is the ability to reproduce, independently, a previous frequency value. Stability, which is the area of most interest in frequency standard development, is the time domain behavior (i.e., variations in frequency over time) of a process. Measured frequency stability depends also on the exact

measurement procedure used to conduct an experiment or evaluation. Frequency stability depends on the tested frequency standard and the measurement system and procedure used. The frequency stability, or instability, of the reference measurement can only be ignored if it is substantially better than that of the tested device. (14:5) For this reason, an HP 5061 Cesium standard was used as the reference frequency standard, which exhibits very good stability characteristics (10^{-14} Hz).

In the time domain, the acceptable measure of stability is the Allan, or two sample, variance. Frequency stability is expressed as the two-sample (Allan) variance, $\sigma_y^2(t)$:

$$\sigma_y^2(t) = 1/2[y_{k+1} - y_k]^2 \qquad 1\text{-}2$$

where the difference in the brackets denotes an average over a number of data points and y_k is the average fractional frequency over time of the data point k. (see Appendix A). The Allan variance is used since frequency measurements in these clock standards do not exhibit a normal distribution. The quantities associated with frequency measurements are the number of measurements (N), the duration of each measurement (τ), and the regular measurement interval (T). The variance $\sigma_y^2(\tau)$ of the process is then defined in terms of the sample variance $\sigma_y^2(N,T,\tau)$ as

$$\sigma_y^2(\tau) = \lim_{N \to \infty} \sigma_y^2(N,T,\tau) \qquad 1\text{-}3$$

when the limit exists. Even after elimination of any initial offset and linear drift, it has been found that the sample variance $\sigma_y^2(N,T,\tau)$ depends on all three variables N, T and τ. Therefore, the sample variance defined in Equation 1-2 has become known among specialists in the time and frequency field as the "Allan-variance". (18:18)

Resonators (14:6-9)

The performance of a frequency standard is given by its frequency determining element. It determines the frequency by its resonance behavior. Some examples of these include: a rod clamped at one end which can vibrate, a block of solid material which can contract and expand (thus vibrate), or an antenna (a dipole) where the distribution of electric charges can oscillate back and forth. These devices have in common that they can vibrate or oscillate if they are excited, by mechanical or electrical stimulation. These excited oscillations will cease gradually with a decay time which is determined by the losses in the individual resonators. Determination of the decay time (t_d) of the oscillations will describe the quality of the resonator. There is also a resonance frequency at which all resonators oscillate at the greatest intensity. On both sides of the resonance frequency, the response of the resonator will lessen until it ceases to respond. There exists a frequency interval around this resonance in which the resonator response is relatively strong and is called the resonance linewidth (W). The relationship between linewidth and decay time is given by:

$$W=1/t_d \qquad 1\text{-}4$$

The fractional linewidth is determined by dividing the linewidth W by its resonance frequency (υ_0). The quality factor, Q, is more commonly used as part of the quality specifications for frequency standards and is the reciprocal of the fractional linewidth:

$$Q=\upsilon_0/W \qquad 1\text{-}5$$

This is graphically represented in Figure 1.1. Large values of Q are required in frequency standards to achieve accuracies in the range of 10^{-12} to 10^{-14}, which implies that the center frequency of the resonance can be determined within a very small fraction of its width.

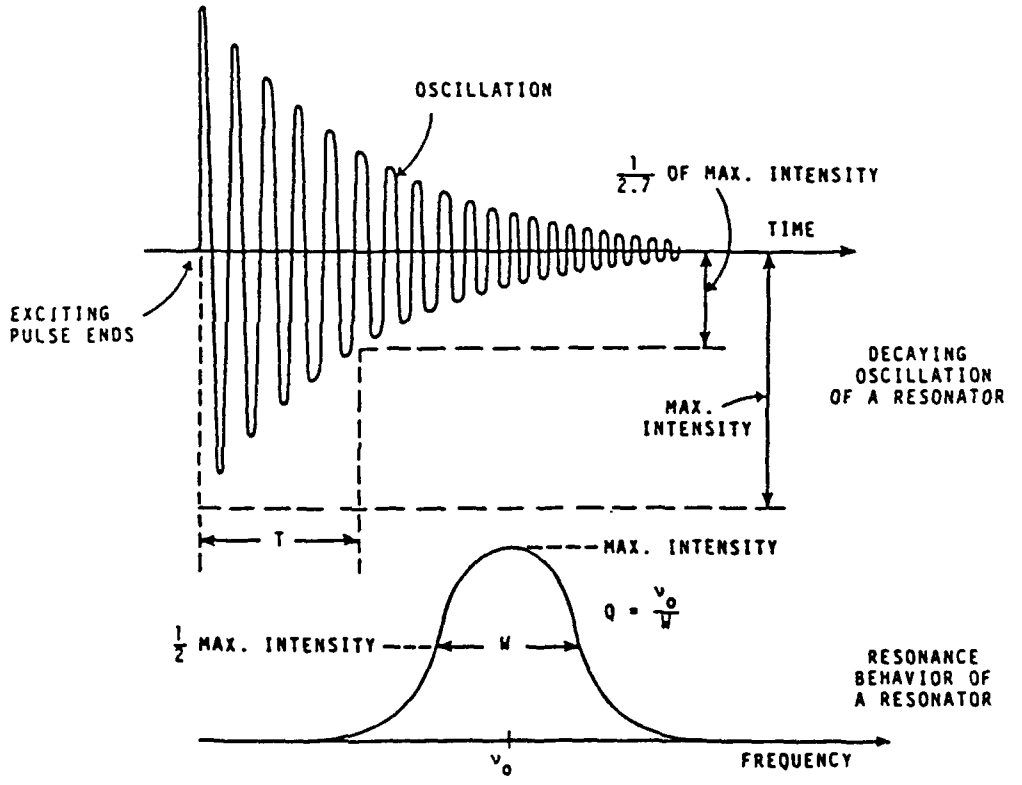

Figure 1.1 Decay Time, Linewidth, and Q-Value of Resonator (14:7)

Quartz Crystal Resonator The quartz crystal is a mechanical resonator which needs an external source to excite its oscillations. This occurs due to the piezoelectric properties of a certain class of crystals. Compression or expansion of the crystal generates a voltage across the crystal and the application of an external voltage across the crystal causes the crystal to expand or contract depending on the polarity of the voltage. (14:9)

An atomic frequency standard is developed from the use of a crystal resonator as the external voltage source, and by adding an electronic amplifier and feedback system back into the atomic resonator. Its output frequency is determined by the quartz crystal resonator whose frequency is determined by the physical dimensions of the crystal combined with the crystalline quartz properties. The nominal output frequencies from the crystal oscillator are 5 and/or 10 Mhz. However, electronic multipliers can be used to provide any desired output frequency. Therefore, a crystal oscillator with a required output of 10 MHz has a crystal thickness of just a few tenths of a millimeter. The output of the crystal oscillator is what is used to drive other systems or used to measure the accuracy of the standard as a whole. (2:3)

Crystal resonators have Q-values which are typically in the range of $Q=10^5$ to 10^7. However, due to external effects such as temperature and acceleration, the crystal resonance accuracy deteriorates more rapidly than is required for space applications. If they are calibrated against high accuracy frequency standards, such as atomic resonators, they maintain this calibration according to their long-term stability performance. (14:16-18)

Atomic Resonators The basis of commercially available atomic frequency standards are resonance in atoms at microwave frequencies, usually in the range of 1 to 100 GHz. An explanation of atomic resonance is compared to

a magnetic dipole antenna. The dipole antennae can be separated into two types, (1) receiving antennae, which absorb energy from a field at their resonance frequency, and (2) transmitting antennae which radiate energy at their resonance frequency. The atoms which act as a receiving antenna are identified as being in the "lower state" and those acting as a transmitting antenna are in the "upper state". This is represented in Figure 1.2. (14:18)

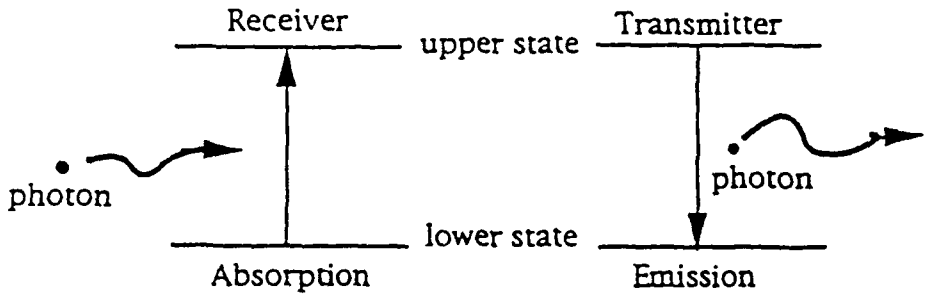

Figure 1.2 Atomic Resonance as Compared to Magnetic Dipole Antenna

The nominal state of most gases have the total number of upper state atoms closely equal to the number of lower state atoms. In actuality though, the probability $P(\varepsilon)$ of finding an entity in one of its variety of energy states ε, for a system containing entities at the same thermal equilibrium, is:

$$P(\varepsilon) = A\, e^{-\varepsilon/\varepsilon o} \qquad 1\text{-}6$$

where A is the state degeneracy constant and ε_o is defined as the quantity $k_B T$. The value k_B is known as the Boltzman constant equal to 1.38×10^{-16} erg/deg and T is the thermal equilibrium temperature of the physical entities of the system.

system. $P(\varepsilon)$ is referred to as the Boltzman probability distribution. At room temperature (~300°K) and a $\Delta\varepsilon$ of about 4.5×10^{-17} ergs between the Rubidium energy states, there is less than a 1% probability difference between finding atoms in the upper or lower energy states. (13:58-61)

If the gas is placed in an external magnetic field, and stimulated by oscillations at the atomic resonance frequency, the atoms will resonate. Nearly half of the atoms absorb energy from the field and the other half emit energy of an equivalent amount to the field. The gas as a whole acts as if it has no resonance, although the individual atoms are resonating. In order to observe the atomic resonance, the relative amounts of each of the states of the atoms must be changed. The upper or lower state has to be in the majority, corresponding to a net absorption or emission of energy. This process determines the design of an atomic resonance device. The frequency of the output is associated with the transitions between these two energy levels. (14:19)

State Selection There are two methods to accomplish the change in the relative number of the two kinds of atoms: 1) spatial state selection and 2) optical state selection. The discussion below is depicted in Figures 1.3 and 1.4, respectively.

Spatial state selection relies on the actual sorting of the two atomic states into different directions in space. One of these states is then used as the resonance standard and the other is discarded. Usually in this case an oven is used to produce an atomic gas by heating it and allowing the atoms to exit the oven through a small hole which forms an atomic beam in an adjacent vacuum chamber. This atomic beam then passes through a magnet which causes the separation of the beam into two separate beams, each of them containing only

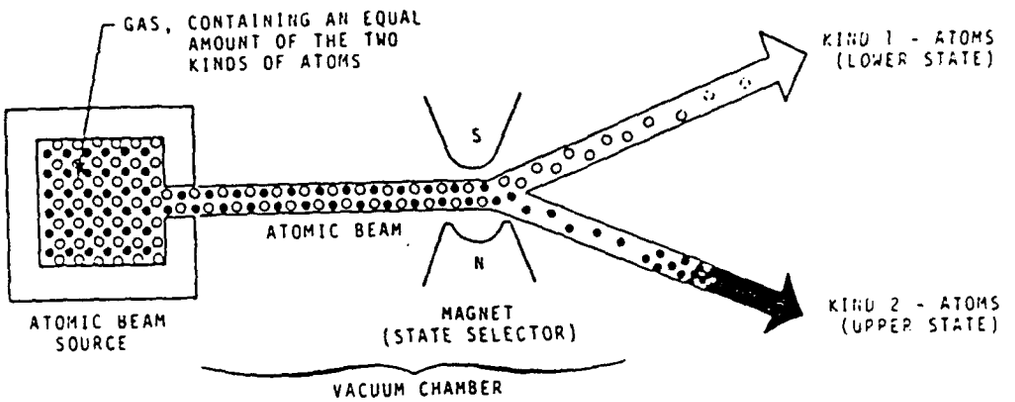

Figure 1.3 Spatial State Selection (14:21)

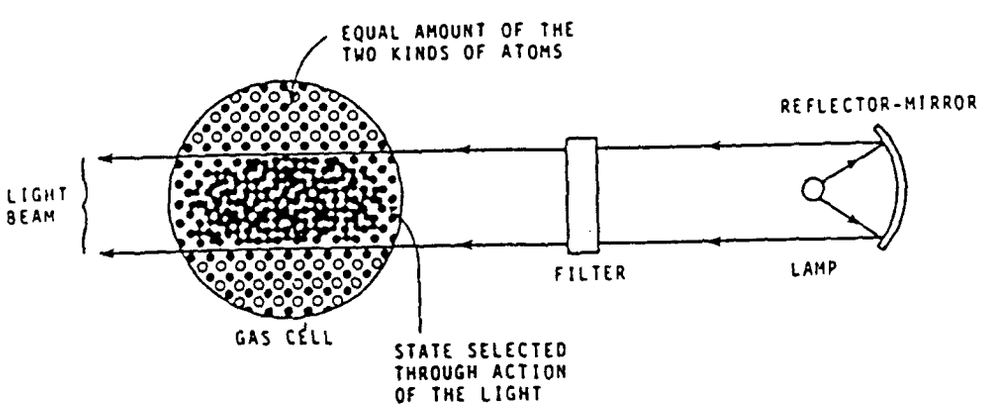

Figure 1.4 Optical State Selection (14:21)

one of the atomic states. This occurs because the magnet will exert a force on these atoms which will act in opposite directions for the two atomic states. This method is usually used in the design of Cesium frequency standards. (14:19-20)

The optical state selection technique takes advantage of the fact that the atoms have more than one resonance. These resonances typically correspond to infrared or visible light frequencies. One of these resonances can be excited by shining an intense light of corresponding frequency on the atoms. These visible light wavelengths for the ^{85}Rb and ^{87}Rb atoms will be discussed in Chapter 2 and how these atoms partially overlapping wavelengths are used to take advantage of a phenomenon referred to as optical pumping. The optical state selection method is usually used in the design of Rubidium frequency standards (14:20).

Atomic Interrogation (14:20-21) A microwave cavity is used to observe the atomic resonance in both of the state selection techniques. These cavities have microwave resonances which are determined by their physical size. The electrical losses of these cavities are determined by the electrical conductivity of the cavity material. These cavities are normally shaped as a cylinder or rectangle, depending on the desired effect. In order to observe the atomic resonance, the state selected atoms are placed inside the cavity and subjected to a microwave signal corresponding to their resonance frequency. The microwave signal will change the the relative number of atoms in the two states. If all the atoms were initially in the upper state, then after the microwave signal has acted upon them there will be lower state atoms produced. If the frequency of the external microwave signal is exactly at the atomic resonance frequency, this transfer of atoms from one state to the other reaches a maximum. The center of the atomic resonance is then found by monitoring

the number of atoms in one of the two states and by varying the microwave frequency until the number of atoms in the lower state reaches a maximum, or the number of atoms in the upper state a minimum. A proportional electric signal is then derived which is fed back to the oscillator generating the microwave signal. This automatic servo mechanism keeps a crystal oscillator locked to the atomic resonance.

Signal Detection (14:22) The detection of the effect of the microwave signal on the atoms is accomplished in three different manners; 1) atom, 2) optical and 3) microwave detection. The optical detection method is the most commonly used in present rubidium standards and will be the only method discussed here. The other methods of signal detection are discussed in detail in Reference 14.

If the atoms are optically state selected, a photo-detector is placed in a position such that the light which has interacted with the atoms is detected. Since the light, which enters the cavity at the same wavelength, removes atoms from one of these states, the light intensity will change when it exits the cavity. This occurs since the atoms in the cavity will absorb the energy of the light photons and decrease its intensity as the light strikes the photodetector. The light at the photo-detector is then a measure of the number of atoms in one of the states, due to the light intensity change. Figure 1.2 graphically depicts how the energy of the light photon can move atoms from one state to another. As was seen in Figure 1.3, the optical wavelengths of the two popular types of rubidium have a very close visible spectrum and this natural phenomenon is taken advantage of in the design of rubidium clocks and will be explained in Chapter II in the optical pumping section.

Fractional Frequency (23:4-5) In providing information regarding frequency accuracy or stability for a given device, the most common method has been termed fractional frequency. Fractional frequency is a dimensionless quantity which determines an error from some known or standard frequency value. In most applications of frequency standards, the output frequency used to drive other devices is not the atomic clock resonance frequency. Electronic frequency multiplication or division is applied to provide a more standardized value, such as 5 or 10 Mhz. Because of these possible applications, absolute frequency values are rarely used. The term *fractional frequency (y) has been* adopted to provide a common basis of world-wide discussion, and is given by the relationship

$$y = (\upsilon_m - \upsilon_n) / \upsilon_n \qquad 1\text{-}7$$

where υ_m is the measured frequency value and υ_n is the nominal value expected. The term "fractional", though in common use throughout the English speaking world, is being discouraged by the Committe Consultatif Internationale de Radio (CCIR), because of the difficulties in translating that term into certain other languages. The CCIR prefers the use of "relative" or "normalized". Results of the experiment conducted here will be provided in terms of fractional frequency, but the above comment should be noted.

Rubidium Clock Principle of Operation

The rubidium system is composed essentially of an optical package acting as a frequency reference, and of a frequency-locked loop for locking the

frequency of a crystal oscillator to the optical package reference as depicted in Figure 1.5. The optical package consists of a ^{87}Rb lamp, a ^{85}Rb hyperfine filter, a ^{87}Rb absorption cell, a microwave cavity and a photodetector. A solenoid is used to create a weak magnetic field inside the absorption cell, which is usually encased in magnetic shielding to attenuate the effect of external magnetic field fluctuations. (2:1259)

Light from the ^{87}Rb lamp, filtered by the ^{85}Rb hyperfine filter, is focused on the absorption cell containing ^{87}Rb and the buffer gas. The lamp consists of a small glass envelope approximately 1 cm in diameter, containing about 0.5 mg of ^{87}Rb and argon at a pressure of approximately 2 Torr. It is excited by an oscillator delivering a power of 1 Watt at a frequency of 80 MHz and heated to a temperature of 125° C. The spectrum of light emitted consists mostly of the D1 and D2 lines of ^{87}Rb as seen in Figure 1.5. As a fact of nature, one of the ^{85}Rb wavelength lines is very closely coincident with one of the ^{87}Rb wavelength lines. (2:1260)

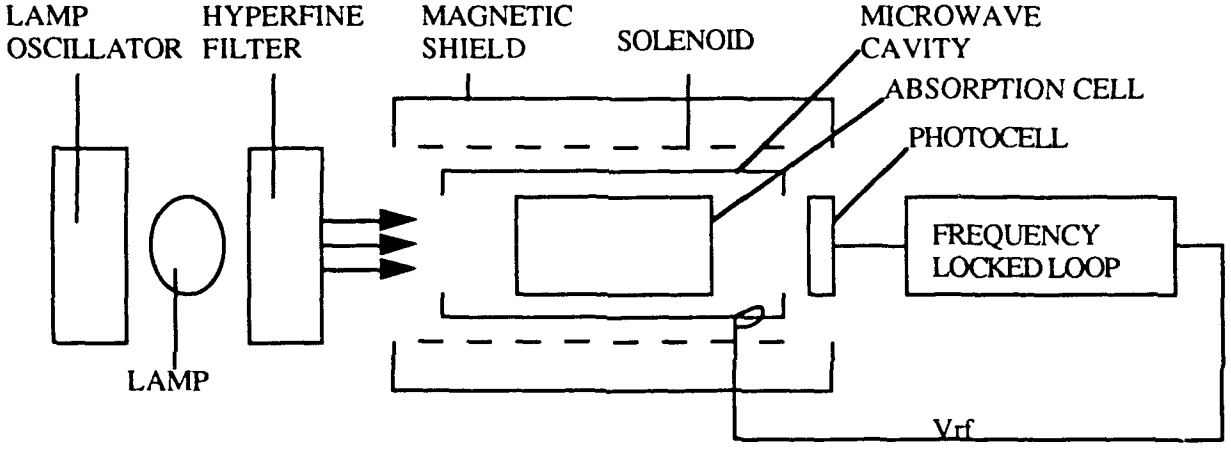

Figure 1.5 Rubidium Frequency Standard Block Diagram (2:1260)

The emitted light is allowed to pass through the hyperfine filter containing the ^{85}Rb plus the buffer gas. The closely spaced optical spectrum lines of the two gases is why rubidium is used in atomic frequency standards, and is exploited for filtering the ^{87}Rb spectrum. The filter cell contains an argon buffer gas which slightly shifts the ^{85}Rb spectrum towards the red wavelength and broadens the lines which make up the overlap to upper wavelength. This increases the efficiency of the filter. When the resulting light, after going through the filter, enters the absorption cell containing additional ^{87}Rb, only atoms in the ground state, which are resonant with the state of interest, are then affected. These atoms are excited to a higher energy state. (2:1261)

Through spontaneous emission or relaxation by collisions with the buffer gas in the absorption cell, the atoms fall back to the ground state. Since the process of excitation is continuously done from the lower ground level (F1), the effect is to increase the population of the level F2 at the expense of the F1 level, which in turn provides an atomic population imbalance between these two states. This effect is known as optical pumping. (9:599-600)

Referring to Figure 1.6, the net result of the optical pumping from the lamp is to overpopulate F2 with respect to F1. Then a microwave radiation at the frequency corresponding to the F2 to F1 (m_f=0 to m_f=0) transition is applied (theoretically 6.834826128(5) GHz), moving the atoms back, toward equilibrium. When the microwave frequency is exactly on the resonance value of a specific absorption cell, then the total light transmitted through the absorption cell to the photodetector is at a minimum. (2:1263)

A constant magnetic field is applied to the absorption cell to keep these ground-state energy levels apart. It was determined by Robert H. Dicke of

Princeton University, that if the container held only rubidium atoms, the Rb irregular thermal motion would cause a condition known as a Doppler shift. This effect shifts the resonant frequency by a different amount for each atom, thus smearing out the resonance line. (5:78)

The accuracy of the standard depends on the relationship between the magnetic field and the position of the levels. Frequency stability of the standard depends on the size of the magnetic field perturbations and the ability to control the field. In order to excite the transitions, a constant magnetic field must exist at the site of the atom and must be parallel to the RF field which excites the transitions. (2:1260)

EG&G Model RFS-10 Description (19:1-1 to 4-8)

The RFS-10 rubidium clock manufactured by EG&G Frequency Products in Salem, MA. is basically a crystal oscillator locked to an atomic

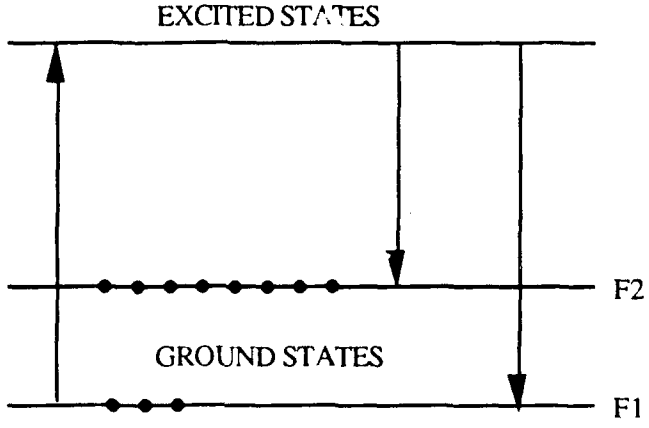

Figure 1.6 State Transitions

reference. A cross sectional view is shown in Figure 1.7. The rubidium physics package serves as a passive discriminator, producing an error signal that varies in magnitude as a function of the difference in frequency between the applied rf excitation and the atomic resonance. The rubidium frequency is about 6835 MHz, with a Q of 10^7. The error signal is a result of an FM audio frequency (~500 Hz) applied to the microwave excitation, which causes variations in the transmission of light through the resonance cell. A photodetector senses this response, which has a typical signal-to-noise ratio of 70 dB, in a 1 Hz bandwidth.

The physics package operation is supported by an exciter for the rubidium lamp and temperature controllers for the lamp and cell ovens. The error signal is processed by a servo-amplifier, which generates a voltage that controls the frequency of a crystal oscillator. This oscillator produces the output and also, via a synthesizer and multiplier chain, drives the physics package. The overall scheme is that of a frequency locked loop.

The RFS-10 resonance cell consists of two devices, a filter cell and an absorption cell. This arrangement generally gives better performance than if the two functions were performed by a single integrated cell.

The RFS-10 rubidium physics package is contained inside a 1.3 inch diameter cylindrical magnetic shield about 2.6 inches long.

Dimensions (19:1-4)

The RFS-10 Rubidium Frequency Standard is a miniaturized high-performance unit measuring 2-3/4 inches by 2-3/4 inches by 4 inches. It features low operating power (12 watts at 25 degrees C), fast warm-up (5 minutes at 25 degrees C), and ruggedized design for military applications.

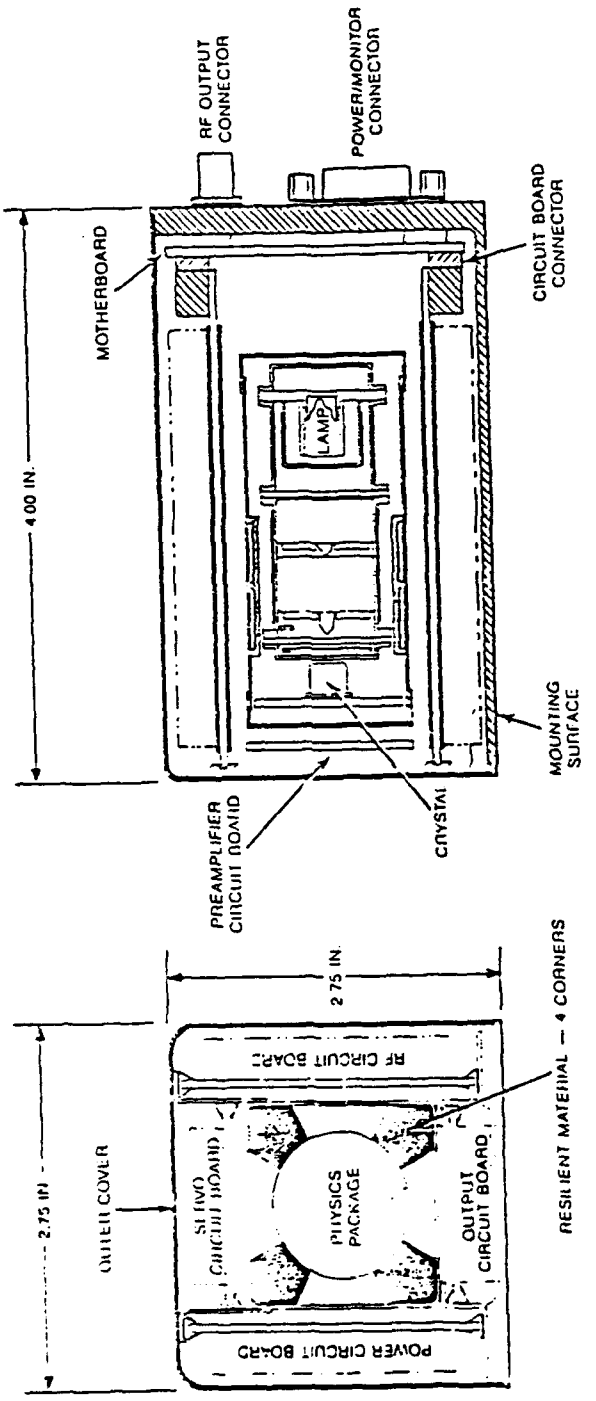

Figure 1.7 RFS-10 Cross Sectional View (19:2-2)

The RFS-10 also features double-shielded construction for low magnetic sensitivity. The lamp and cell ovens have low thermal mass to aid in fast warm-up.

The RFS-10 has two ovens that control the temperature of elements inside the rubidium physics package. One oven heats the rubidium lamp and the other heats a microwave cavity which contains the filter and absorption resonance cells and also holds a crystal oscillator.

Physics Package Description (19:4-3)

The physics package assembly is comprised of the following major elements: 1) lamp exciter, 2) lamp oven, 3) microwave cavity, 4) photodetector, 5) crystal oscillator and 6) preamplifier. A cross sectional view of the physics package is depicted in Figure 1.8.

The lamp oven contains the rubidium lamp. The microwave cavity contains the filter and absorption cells and a microwave multiplier. The heart of the RFS-10 unit is the physics package described in the following pages.

The physics package includes two lenses in the optical path. The first, located in front of the absorption cell, collimates the lamp output to give a uniform light intensity distribution. The second lens, located behind the absorption cell, focuses the light on the photodetector to give good collection efficiency. The photodetector is a custom EG&G device having low noise.

The rubidium lamp is excited with an rf power of about 0.5 watt at 105 MHz. This energy is applied to the lamp by operating it inside the field of an rf coil which excites optical emissions from an ionized plasma. The lamp provides

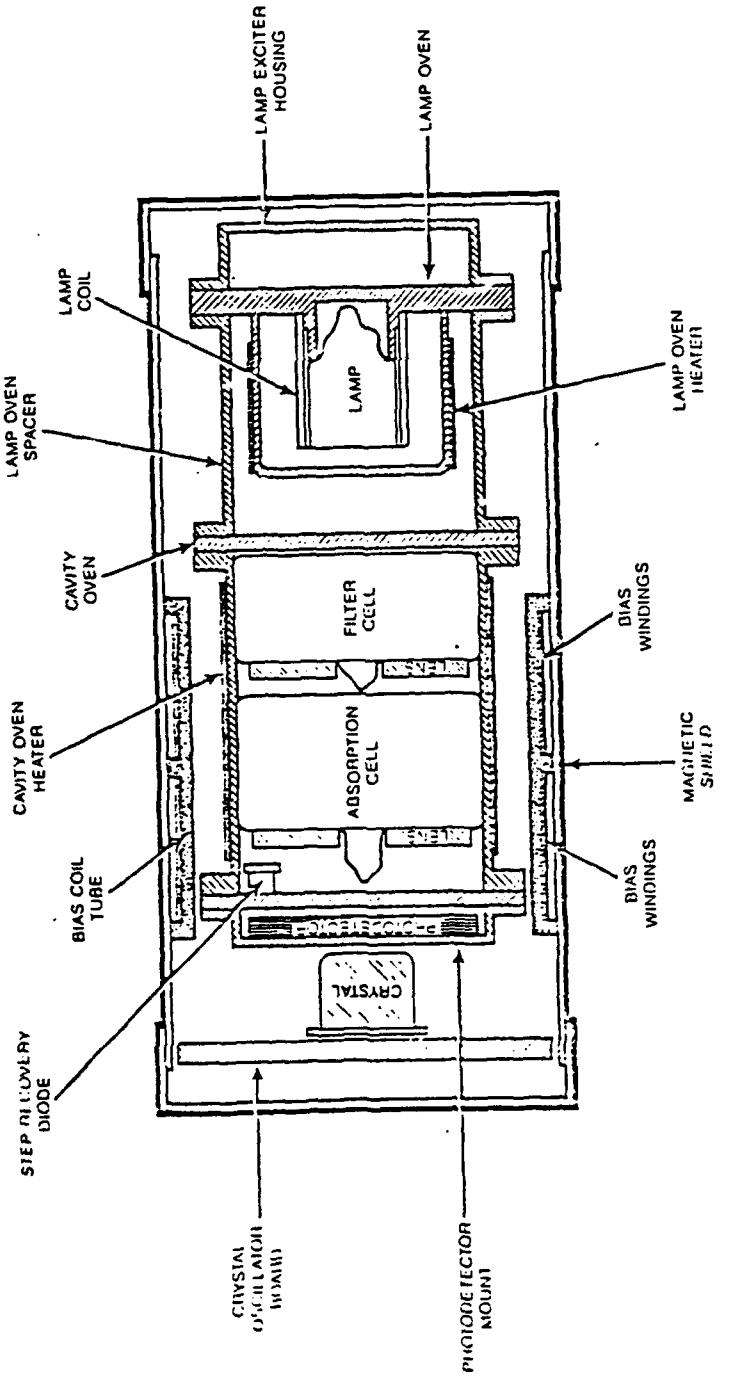

Figure 1.8 RFS-10 Physics Package (19:4-5)

the Rb resonance radiation required for optical pumping.

The step-recovery diode (SRD) microwave multiplier is incorporated into the temperature-controlled cavity. Its design is both simple and efficient since it works as a straight x76 multiplier. It is driven by a +20 dBm signal at about 90 MHz and produces about 100 micro-watts at the rubidium resonance frequency of approximately 6835 MHz.

The VCXO board is located inside the physics package assembly. It consists of a 20 MHz voltage-controlled crystal oscillator (VCXO) that is locked by the servo-amplifier to the rubidium resonance frequency and produces the output signal from the RFS-10. The VCXO uses a 20 MHz fundamental mode SC-cut crystal. This crystal type is chosen for its small size, fast warm-up, and low vibration sensitivity. It is mounted on the 1.25 inch diameter VCXO board that is attached to the photodetector end of the microwave cavity and thereby shares the 80 degrees C stabilized thermal environment of the cavity oven.

Problem Statement and Experiment Approach

There is a close bond between the interaction of the atomic magnetic moment, the external C-field to which it is exposed, and the power associated with the electromagnetic wave which causes the hyperfine transitions.

As evident in experiments conducted by Andrea DiMarchi (12:54-58), the cesium frequency standard can be improved in long-term frequency stability by the correlation of absorption cell magnetic field values versus the microwave power used to excite the cesium hyperfine transitions. His experiment and analysis concluded that there were certain magnetic field values which minimized any frequency shifts in the output of the cesium clock

due to any changes in microwave power. Variations in microwave power could result in external effects on the clock electronics which would make it difficult to control when used in space applications. His recommendation was to adjust, or tune, the cesium cavity to one of several specific magnetic field values, which in turn improved the long term accuracy of the clock (11:517-521).

Since similar experiments have not been performed on rubidium clocks, this paper will parallel the experiment conducted by DiMarchi, except using a commercially available rubidium standard, provided by EG&G Frequency Products. Results, analysis and conclusions will be provided as to the outcome of this experiment.

The objective of this experiment is to gather and analyze applicable data which will provide the necessary information to validate theoretical models and answer the primary question: "Are there magnetic field values which improve (a specific) rubidium clock performance when the microwave power is varied?"

The following questions will be investigated:

1) Does the theoretical model for rubidium hyperfine transitions match the experimental results? What is the error associated with experimental data?

2) The average magnetic field value can be calculated using existing models. Can this model be used to accurately determine the magnetic field inside the absorption cell?

3) Is there a linear or non-linear relationship between Zeeman frequencies and coil magnetic field changes? Explain the relationship.

4) Are there magnetic field settings within the operating parameters of this rubidium clock which minimize output frequency variations to microwave power variations?

5) Is there a relationship between changes in microwave power and changes in the values of the Zeeman frequencies?

6) Is there a relationship between changes in microwave power and the shape of the resonance spike?

II. *Theory*

A basic understanding of the theory of atomic structure and the stability of atoms will be discussed to explain the operational phenomena within Rubidium frequency clocks. The chemical properties of all elements in the periodic table give rise to their suitability for use in accurate long term time measurement applications. Hydrogen, consisting of one single electron orbiting its nucleus, has been studied in detail and gives rise to the most accurate timing standards available. Other elements exhibit a similar characteristic to that of hydrogen. This similarity is the presence of an unpaired electron orbiting the nucleus of the atom, and are known as the alkali elements in the periodic table. These elements have one single electron orbiting around a closed subshell of paired electrons. The resonance of the single orbiting electron is one of the reasons that rubidium clocks are used today. (2:7)

There exists two naturally formed rubidium atoms; one has an atomic weight of 85 and the other 87. Both of these atoms are used together in the design of rubidium clocks. The standard nomenclature to differentiate between these two atoms are the symbols ^{85}Rb and ^{87}Rb. In the case of ^{87}Rb, the nucleus is composed of 37 protons (known as the atomic number), and 50 neutrons. It consists of five shells, or layers, with a total of 37 electrons. Each electron shell is filled through the determination of the individual quantum numbers n,l, and m. The principal quantum number, n, will determine the allowable values for the azimimuthal and magnetic quantum numbers l and m. The quantum numbers can take the following values:

$$n = 1, 2, 3,..., \text{infinity}$$

$$l = 0, 1, 2, ..., (n-1)$$

$$m = -l, -(l-1), ..., +(l-1), +l$$

The particular conditions, regarding the minimum and maximum values that these quantum numbers can take, are set by the eigenvalue equations resulting from Equation 2-2 when the solution for Equation 2-4 is replaced in it. (8: 53)

The representation for the electron distribution for ^{87}Rb is given through the following series arrangement: $1S^2\ 2S^2\ 2P^6\ 3S^2\ 3P^6\ 3D^{10}\ 4S^2\ 4P^6\ 5S^1$. The numbers in front of the letters indicate which orbiting shell the electrons are found in (related to the principle quantum number n); the letters represent the electrons angular momentum (related to the value of l) ,and the superscript identifies the number of electrons in that subshell composition. Each of these states correspond to a different energy level.

The ^{87}Rb electron distribution above indicates that the last shell ($5S^1$) contains an unpaired electron as seen in Figure 2.1. Movement of this electron through some type of stimulation, allows it to move to another energy state. As will be seen in this chapter, the movement between these energy states corresponds to different frequency values. Figure 2.1 also represents an exaggerated view of this electron and the next two energy states (5P) in which this electron could be moved. The subscripts in this figure represents the designation for the total angular momentum due to electron-nucleus interactions, and will be discussed in more detail. The D1 and D2 designation in the figure represents the optical wavelength associated with the movement of the electron between these two states.

The interaction between the electron and the nucleus plus the effects which occur due to outside stimulation will be briefly discussed in this chapter

to provide a better understanding of what is occurring at the atomic level to provide the results of this study.

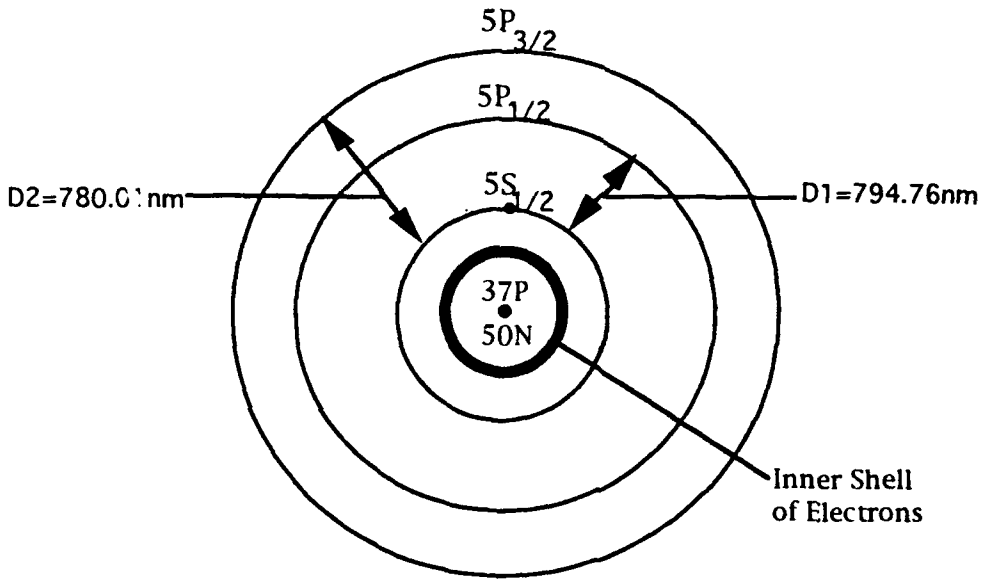

Figure 2.1 ^{87}Rb Unpaired Electron Configuration

Atomic Spectra

The field of atomic frequency standards is characterized by a level of accuracy that is not seen in other fields of physics and engineering. This accuracy relies partly on the existence of calculations of various perturbations which influence the properties of the atoms of interest. As errors in the neighborhood of 10^{-14} are being investigated, precise measurements, procedures and calculations need to be performed. A brief discussion on atomic spectra, as well as some details on rubidium, will follow to orient the reader as to why some phenomena occur when atoms are subjected to certain stimuli.

Principal Quantum Number An electron in an atom moves about the nucleus under the influence of the Coulomb attraction between the electron and the nucleus. The potential energy of this closed system is given by:

$$V(r) = -e^2/ 4 \pi \varepsilon_o r \qquad 2\text{-}1$$

The Schroedinger time-independent wave equation is determined from the following relationship: (10:7-4)

$$((- h^2 / 2 \mu \nabla^2) - (e^2 / 4 \pi \varepsilon_o r)) u(r, \theta, \phi) = E u(r, \theta, \phi) \qquad 2\text{-}2$$

where u (r, θ, ϕ) is the wavefunction in spherical coordinates, independent of time, μ is the reduced mass expressed as:

$$\mu = M_p m / (M_p + m) \qquad 2\text{-}3$$

and M_p is the mass of the proton and m is the mass of the electron. In expression 2-2, E is the total energy of the atom assumed at rest, r is the electron-proton distance, ε_o is the permittivity of free space, e is the electron charge and ∇^2 is the Laplacian operator.

The solution of this equation can be obtained by expressing ∇^2 in terms of spherical coordinates. The variables are separated and the wavefunction $u(r, \theta, \phi)$ can be written in terms of Laguerre polynomials, R, and spherical harmonics, Y. Several functions, $u(r, \theta, \phi)$, characterized by the quantum numbers n, l, and m are obtained:

$$u_{nlm}(r, \theta, \phi) = R_{nl}(r)\ Y_{lm}(\theta, \phi) \qquad 2\text{–}4$$

The normalized spherical harmonic $Y_{lm}(\theta, \phi)$ can be written in terms of the normalized associated Legendre polynomial P_{lm} as

$$Y_{lm}(\theta, \phi) = [1/(2\pi)^{1/2}]\ P_{lm}\ e^{im\phi} \qquad 2\text{–}5$$

The principal quantum number, n, is generated by the solution of the radial part of the equation. It gives rise to the energy levels: (10:7-4)

$$E_n = -(\mu\ e^4)/(32\ \pi^2\ \varepsilon_o^2\ h^2\ n^2) \qquad 2\text{-}6$$

Since all items are constants in the energy equation except for n, this can be reduced to:

$$E_n = -E_I/n^2 \qquad 2\text{-}7$$

where E_I is the atom's ionization energy. For Rubidium, E_I = 4.177 eV (electron-volts) where 1 eV = 1.5956 x 10^{-12} ergs. The lowest energy (the most negative) is that in which the principle quantum number n equals 1, which is called the ground state. (25:924-925)

Each energy level corresponds to a stationary state in which the atom can exist without radiating. Stationary states above the ground state (n = 2, 3, 4, ...) are called the excited states. An electron in one of these states tends to make a transition to one of the lower stationary states. (25:925)

An electron, initially moving in an excited state of total energy E_i, changes its motion such that it moves into a lower state of total energy E_f. In the transition, the atom losses energy $(E_i - E_f)$, where a single photon having energy $h\upsilon$ is created and emitted by the atom. The frequency of the emitted radiation υ is equal to the difference between these energy levels divided by Planck's constant, or:

$$\upsilon = (E_i - E_f)/h \qquad 2\text{-}8$$

Therefore, υ would be considered a constant, only dependent on the two levels chosen in the energy scheme of the atom. (15:773)

Equation 2-8 assumes that the atoms are at rest. However, atoms are continuously in motion and their emission and absorption frequencies are functions of their velocity relative to the observer. Since the atomic velocities are random, with a Maxwellian distribution (2:451), the net effect is that each atom emits or absorbs energy at slightly different frequencies, referred to as Doppler broadening. The net frequency result, υ_o, called the resonance frequency, is spread over a broad range. The half power frequency width of this doppler effect is given by:

$$\Delta\upsilon_D = 2\,\upsilon_o\,[\,(\,2\,k_B\,T/\,M\,c^2\,)\,\ln 2]^{1/2} \qquad 2\text{-}9$$

where M is the rest mass of the atom, and the other variables have been previously defined. In the case of optical spectra, the frequency width $\Delta\upsilon_D$ can be very large due to the fact that υ_o is high. In the case of the ground-state hyperfine transition in Rubidium at room temperature, the width is

approximately 3 KHz. The principle behind an atomic frequency clock is to reduce this broad range of frequencies to a very stable value with extremely small perturbations, in the short or long term, from the resonance value. Accurate controlling of this frequency provides the timing accuracy and stability required in modern time devices. (13:468-472)

The following sections are only approximate descriptions of the classical quantum mechanics associated with a multiple electron atomic configuration, and are provided to aid the reader in visualizing the relationships of angular momentum, magnetic moments, and internal atomic magnetic field interactions. The unpaired electron in rubidium is the one of interest as compared to the single hydrogen atom, but there other relativistic effects from the inner shell electrons which contribute to its behavior.

Orbital Angular Momentum (25:930-931) The motion of the electron around the nucleus in these variety of orbits possesses an orbital angular momentum. In the ground state, where the electron orbit is circular, the orbital angular momentum is zero. The magnitude of the electron's angular momentum, L, is represented in terms of the orbital angular-momentum quantum number, l, and is given by:

$$L = [\, l\,(\,l + 1)\,]^{1/2}\, \hbar \qquad 2\text{-}10$$

where $\hbar$ is Planck's constant (h) divided by 2π. The value of l may take on integral values starting with zero and continuing up to (n-1), where n is the principle quantum number. Each value of l corresponds to a state. The case of l equal to zero is where the electron has no orbital angular momentum

relative to the nucleus and is considered to be in the S state. The next values of l (1,2,3,4...) correspond to the states P,D,F,G,..., respectively.

When a single electron undergoes a transition from one allowed state to another, and a photon is emitted, that state can only change such that the value of l changes by the integer 1, or Δl equals +/- 1.

Orbital Magnetic Moment (13:327-329) Associated with the orbital angular momentum vector of the last section is the orbital magnetic moment μ_l. From electromagnetic theory, the electron charge circulating in a loop will generate a current. In addition, such a current loop produces a magnetic field which is the same at large distances as that of a magnetic dipole located at the center of the loop and oriented perpendicular to its plane.

For a current i in a loop of area A, the magnitude of the magnetic moment of the equivalent dipole is:

$$\mu_l = iA \qquad 2\text{-}11$$

Figure 2.2 is a representation of the angular magnetic moment vectors. The magnetic moment is a measure of the strength and orientation of the dipole. The abbreviations np and sp relate to the strength of the positive pole (np) and the negative pole (sp).

For a current loop produced by a negatively charged particle, the direction of μ_l is opposite the direction of the angular momentum vector L. Also, the ratio of the magnetic moment to the magnitude of the angular momentum is a constant known as:

$$\mu_l / L = g_l \mu_B / h \qquad 2\text{-}12$$

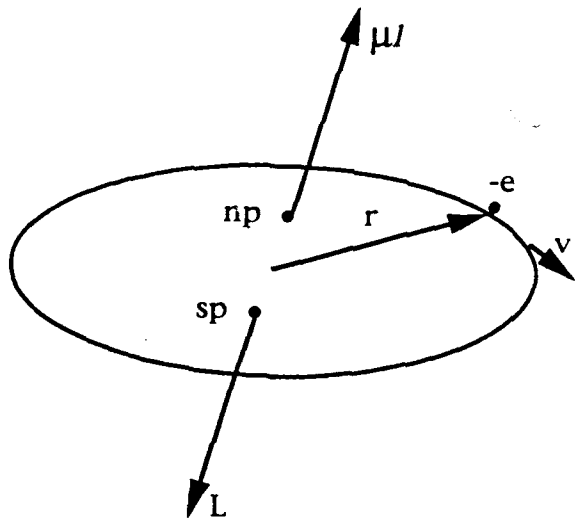

Figure 2.2 Vector Representation of Orbital Angular Momentum Vector L and Associated Magnetic Moment Vector μl (13:328)

where μ_B, called the Bohr magneton, forms a natural unit for the measurement of atomic magnetic moments. The quantity g_l is called the orbital g factor, with a value approximately equal to one.

The magnetic moment can be written in terms of the orbital angular momentum:

$$\mu_l = - (g_l \mu_B / h) \mathbf{L} \qquad 2\text{-}13$$

The ratio of of these two vectors does not depend on the size or shape (circular versus elliptical) of the orbit nor on the orbital frequency.

Equation 2-10 provides the magnitude of the angular momentum as a scalar, but the direction was not identified. The orbital magnetic quantum number m_l yields the component of the electron's orbital angular momentum,

relative to some arbitrary direction in free space, which will be called z. The values of m_l range from + l to - l. Figure 2.3 represents the magnitude, direction, and z-component of the angular momentum vector associated with an electron in the D state (l = 2).

Since the value of the z-component of the angular momentum vector can be represented in terms of the quantum number m_l, then by Equation 2-13 the magnetic moment vector in the z-direction can also be represented in terms of the same quantum number:

$$\mu_{lz} = - g_l \mu_B m_l \qquad 2\text{-}14$$

As seen in Figure 2.3, Lz = $m_l h$ with m_l an integer, and since the direction of the z axis was chosen arbitrarily, then the quantum mechanics

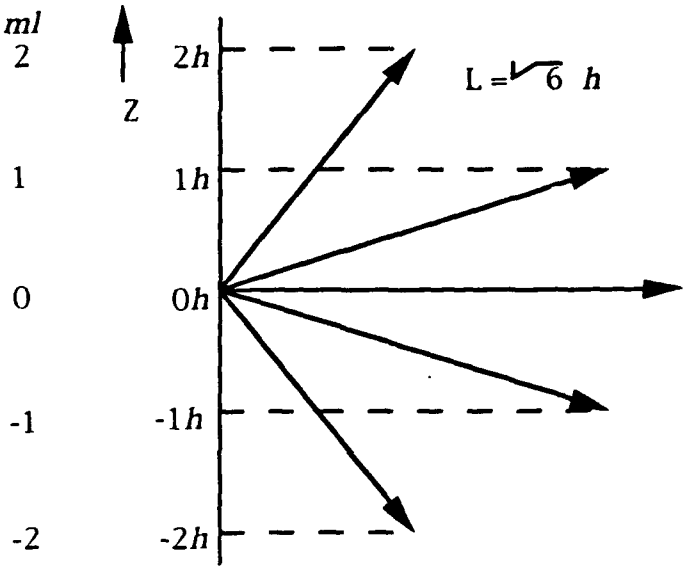

Figure 2.3 Representation of Orbital Angular Momentum Vector L and Orbital Magnetic Quantum Number m_l for D State (25:932)

requires the component in any direction of the orbital angular momentum to be an integral multiple of h. This is known as spatial quantization.

Atomic Magnetic Field Effects. (13:330-331) If the dipole represented in Figure 2.2 is subjected to an external magnetic field H in the z direction , then there will be a force acting on the positive and negative poles (np and sp). In this external magnetic field a force of magnitude spH will act on the positive pole (np), with an equivalent, but oppositely directed, force acting on the negative pole (sp). There is no net translational force, but there will be a torque applied to the center of the structure. The magnitude of the torque will also depend upon the angle between the magnetic moment μ_l and the vector H_z. The magnitude and direction of this torque can be expressed through the cross product of the two vectors:

$$\mathbf{T} = \mu_l \times \mathbf{H} \qquad 2\text{-}15$$

Therefore, with this orientation torque, the atomic system will have an orientation potential energy, ΔE, dependent only on the angle between the two vectors. This ΔE can be written in terms of the dot product:

$$\Delta E = - \mu_l \cdot \mathbf{H} \qquad 2\text{-}16$$

This orientational potential energy is minimized when the two vectors are aligned. Since there is no internal mechanism to allow for a dissipation of energy, then the magnetic moment will precess around the external magnetic field vector in such a way that the angle between the vectors and ΔE will remain constant.

This precessional motion is a consequence of the torque always being perpendicular to the angular momentum vector **L**. Equation 2-16 can be written in terms of **L**, from what was derived in Equation 2-13. Therefore **L** and μ_l will precess about **H** with an angular frequency of magnitude ω_L and can be represented as:

$$\omega_L = (g_l \mu_B / h)\, \mathbf{H} \qquad 2\text{-}17$$

This is known as the Larmor frequency and is graphically represented in Figure 2.4.

Electron Spin (13:334-338) In addition to the angular momentum due to an electron orbiting the nucleus, it also has an intrinsic angular momentum due

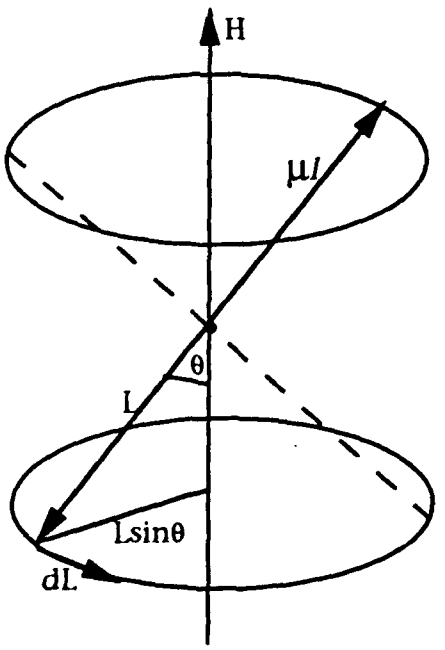

Figure 2.4 Magnetic Moment Vector μl Precessing About External Magnetic Field H (13:332)

to the existence of the electron spinning. The magnitude of this spin angular momentum, S, is related to the spin quantum numbers s. The equation for the angular momentum magnitude is the same as that for the orbital angular momentum vector (reference Equation 2-10) and given by:

$$S = [\, s\,(s+1)\,]^{1/2}\, h \qquad 2\text{-}18$$

The relationship between the spin angular momentum and the spin magnetic moment is the same as before and can be written as:

$$\mu_S = -\,(g_S\, \mu_B / h)\, S \qquad 2\text{-}19$$

where g_S in this case is called the spin g factor, which is approximately equal to two. The actual value of g_S for Rubidium is 2.002331. (2:24)

Since the value of the z-component of the angular momentum vector can be represented in terms of the quantum number m_S, as in Equation 2-14, then the magnetic moment vector in the z direction can also be represented in terms of this spin quantum number:

$$\mu_{Sz} = -\, g_S\, \mu_B\, m_S \qquad 2\text{-}20$$

Due to the fact that the axis of rotation does not change, it can be seen that the z-component of the magnetic moment for a single electron atom will only assume two values, which are equal in magnitude but opposite in sign. The spin quantum number m_S can only have the values +/- 1/2 and s can only have a single value equal to 1/2.

The spin angular momentum and the magnetic moment are opposite in direction, as were the orbital angular momentum and the orbital magnetic moment (seen in Figure 2.4).

The atomic system will also have an orientational potential energy contribution due to the spin magnetic moment. This ΔE can be written in terms of the dot product:

$$\Delta E = - \mu_s \cdot H \qquad 2\text{-}21$$

Total Electronic Angular-Momentum (13:346-353) The orbital angular momentum L plus the spin angular momentum S, form the total electronic angular momentum J:

$$J = (L+S) \qquad 2\text{-}22$$

For simplification then, the quantum number m_j was formed to represent the sum of the two other quantum numbers, m_l and m_s, which will be reduced when substituting in the values for the orbital and spin angular momentum vectors into Equation 2-22. Since the maximum possible value of m_l is l, and the maximum possible value of m_s is s=1/2, then the maximum possible value of m_j is (l + 1/2). In the ground state, where L=0, it can been seen that J = S, therefore, m_j equals +/- 1/2, and for j it is equal to 1/2.

The electron spin-orbit interaction energy contributions were directly related back to the quantum numbers n and j to produce the equation which identifies the atomic *fine structure* for hydrogen atoms only:

$$E = - (\mu Z^2 e^4 / 2n^2 h^2) [1 + (\alpha^2 Z^2 / n)(1/(j+1/2) - 3/(4n))] \qquad 2\text{-}23$$

where α is called the *fine structure constant*, equivalent to approximately 1/137 or more exactly (7.29720×10^{-3}) (10:7-27).

This equation determines the energy levels in terms of the electron orbit and received consistent results with Bohr's findings, when the electron's orbits were assumed to be circular in the calculation for the state energy values. As can be seen in Figure 2.5, the number of energy splits at each level is related to the principal quantum number n. This also identifies the only permitted energy level transitions between these energy splits, which is consistent with the explanation of the quantum number *l* discussed earlier. These *fine* lines are greatly exaggerated for representation purposes. The difference between these lines at each energy state level is on the order of α^2. The arrows indicate transitions between the various energy states allowed which produce the lines of the atomic spectrum.

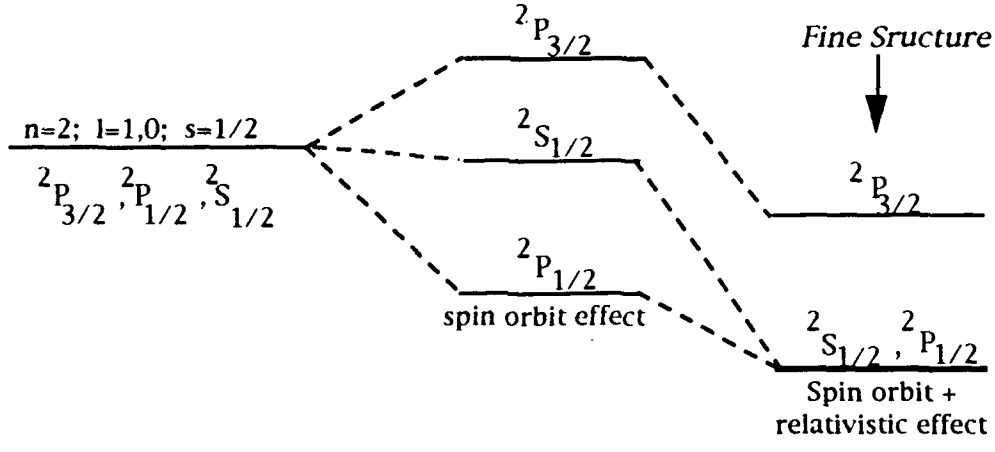

Figure 2.5 Splitting of the n=2 Levels by the Spin-Orbit Coupling Plus Relativistic Effect

Zeeman Effect(13:443-448)

It has also been observed that placing an atom, such as the alkali atoms, in an external magnetic field contributes to what is now called the Zeeman effect. This effect is an observation that the spectral lines produced due to the fine structure are also separated into several components. For external fields up to a few thousand gauss, this splitting is proportional to the strength of the magnetic field, but is small in comparison to the fine structure splitting of the spectral lines of the atoms. This also means that in the presence of a magnetic field, the energy levels of the atom which contribute to the spectral lines must then also be split into several components.

Earlier it was discussed (page 2.12) that the summing of the electrons orbit and spin angular momentum resulted in the total angular momentum vector **J**. So it follows that in the presence of the same magnetic field **H**, that the energy difference can also be represented as:

$$\Delta E = - \mu_H H \qquad 2\text{-}24$$

where μ_H is the component of the total magnetic moment along the direction of H.

The Larmor precession that existed with the angular momentum and magnetic moment vectors in Figure 2.2 also holds true for the spin angular and magnetic moment vectors. In this case, however, **L** and **S** precess about **J** because of the precession of **S** in the atomic magnetic field associated with **L**, and have a precessional frequency w_L. This precessional frequency is proportional to the strength of the atomic magnetic field. The total magnetic moment vector μ, will also precess about **J** with the same precessional

frequency. In the presence of an external magnetic field H, there will also be a precession of μ about the direction of this field with a *precessional frequency* proportional to the strength of H. If the external field is weak compared to the atomic magnetic field, then the precession of μ about **H** will be slow compared to the precession about **J**. This is graphically represented in Figure 2.6.

All cases discussed in this paper assume that the external magnetic field is considerably smaller than the atomic magnetic field. The value of the atomic magnetic field has been measured to be on the order of 10^4 gauss.

Since μ precesses much more rapidly about **J** than about **H**, μ_H can be evaluated by looking at μ_J. Therefore, μ_H can be represented in terms of μ_B and the quantum number m_j. The resultant average energy difference can then be written as:

$$\Delta E = \mu_B \, H \, g \, m_j \qquad 2\text{-}25$$

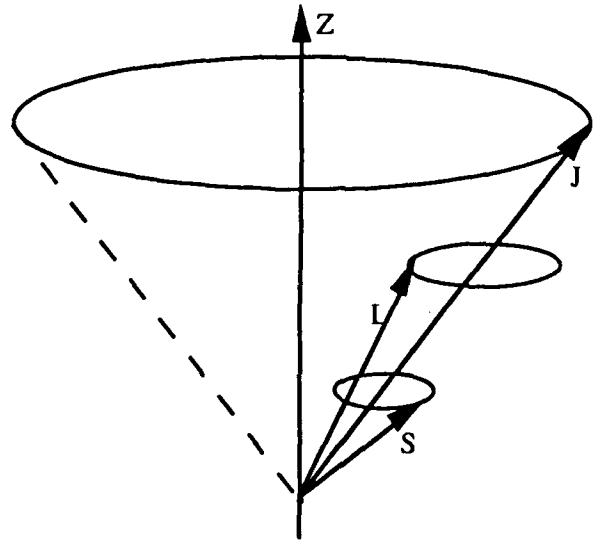

Figure 2.6 Electron S and L Angular Momentum Vectors Precessing about J which Precesses about Z

The quantity g is called the Lande g factor and is composed of the quantum numbers s, l, and j, and evaluated through the expression:

$$g = 1 + [\, j(j+1) + s(s+1) - l(l+1)] \,/\, 2j\,(j+1) \qquad 2\text{-}26$$

The net effect of this is graphically represented in Figure 2.7. The vertical lines indicate the only allowed state transitions between energy levels and follow the earlier defined optical selection rule (page 2.12) of Δm_j=0 and +/-1. The S state in Figure 2.7 refers to the ground state where the quantum number n=1, therefore l=0, and the subscript 1/2 refers to the only value that j can assume, which is 1/2. For the P state, n=1, therefore l can have values of both 0 and 1. From this, the subscript of 1/2 and 3/2 relates to the two possible values of j.

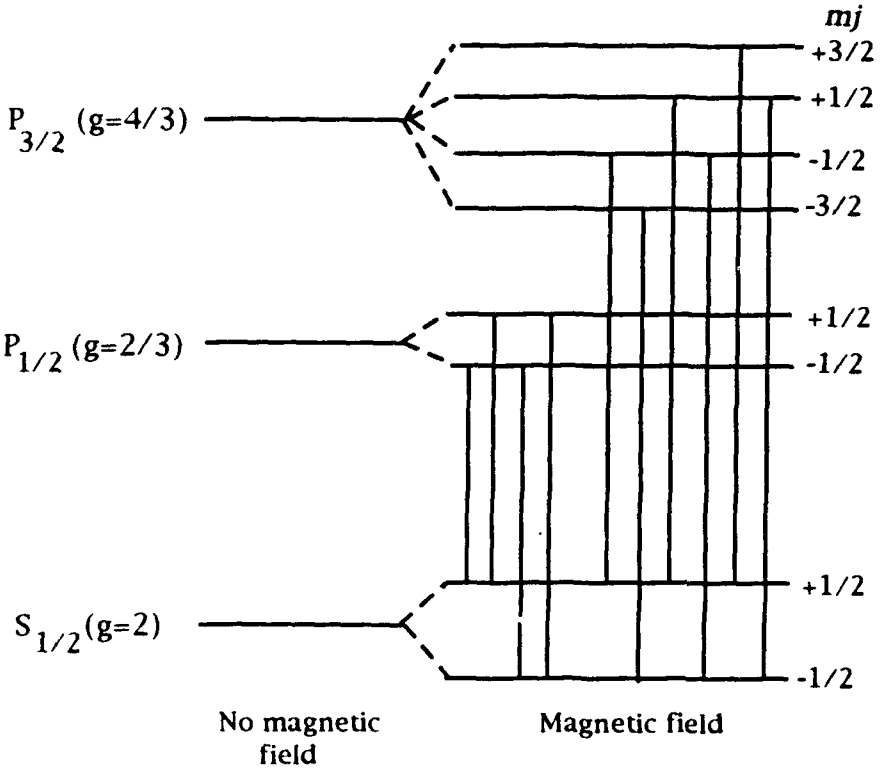

Figure 2.7 Zeeman Splitting of Typical S and P Energy Levels (8:237)

Hyperfine Structure (13:449-452)

In addition to the splitting of the spectral lines associated with the *fine* structure, there are additional separation components that arise due to the effect of the nucleus spinning. These lines are very closely spaced and are on the order of three orders of magnitude smaller than the separation characteristics of the fine structure of spectral lines. These small components are referred to as the *hyperfine* splitting of the energy levels of the atom.

This hyperfine splitting is a result of the orientational potential energy of the magnetic dipole moment due to the atomic nucleus interacting with the magnetic field associated with the motion of the electrons. The nuclear magnetic dipole moment μ_I is due to the nuclear spin angular momentum, **I**, which is derived in the same manner as the electron spin angular momentum vector, **S**. A representation of both the electron and nucleus angular momentum vectors is depicted in Figure 2.8.

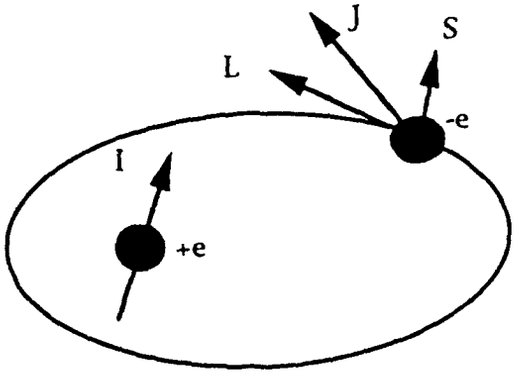

Figure 2.8 Model of Electron and Nucleus Angular Momentum Vectors (8:230)

The magnitude and Z component of I are represented using a new quantum number associated with nucleus spin m_i, and is derived in the same manner as the electron spin angular momentum:

$$I = [\, i\,(i+1)\,]^{1/2}\, h \qquad 2\text{-}27$$

therefore

$$I_Z = m_i\, h \qquad 2\text{-}28$$

The equation relating the nuclear magnetic dipole moment to the nuclear spin is given by:

$$\mu_i = (g_i\, \mu_N / h)\, \mathbf{I} \qquad 2\text{-}29$$

such that

$$\mu_{iz} = g_i\, \mu_N\, m_i \qquad 2\text{-}30$$

The factor g_i is also on the order of 1 (.995141 for ^{87}Rb) (2:25), but is positive for some nuclei and negative for others, depending on the spin direction. The quantity μ_N, which is called the nucleus magneton, is a factor of 1836 smaller than that of μ_B (the Bohr magneton). Since the nuclear magneton is over three orders of magnitude smaller than the Bohr magneton, it follows that the nuclear magnetic moment is smaller than the total electron magnetic moment by the same factor. Consequently the orientational potential energy of the nuclear magnetic moment (hyperfine structure) is three orders of magnitude smaller than the orientational potential energy of the atomic magnetic moment (fine

structure), since both magnetic moments experience comparable magnetic fields.

The interaction of the nuclear magnetic dipole moment with atomic magnetic field couples the nuclear spin angular momentum vector I to the total angular momentum vector J of the electrons. Because of this coupling, a new grand total angular momentum vector is generated, **F**, composed of the sum of **I** and **J**:

$$\mathbf{F} = \mathbf{I} + \mathbf{J} \qquad 2\text{-}31$$

Both the **I** and **J** vectors will now be seen precessing about the grand total angular momentum vector. Consequently, when the hyperfine structure interaction is evaluated, m_i and m_j are not used, but a new quantum number, m_f, is introduced. The relationship between the magnitude and z direction is the same as the earlier sums seen in angular momentum and grand total angular momentum. Grand total angular momentum can now be represented as:

$$F = [\, f\,(f+1)\,]^{1/2}\, h \qquad 2\text{-}32$$

and the z component by:

$$F_z = m_f\, h \qquad 2\text{-}33$$

Rubidium Zeeman Splitting

The effects from the Zeeman splitting for the Rubidium atom discloses that, in the visible light spectrum, this atom produces two primary wavelength

spectrums, referred to as the D1 and D2 lines. They are represented by taking a closer look at the frequencies associated with the transitions between the $P_{1/2}$ and $P_{3/2}$ to the ground state $S_{1/2}$. Figure 2.3 can be expanded and represented by Figures 2.9 and 2.10. These figures represent the state transition frequencies which sum together to give the two optical wavelengths represented by the D1 and D2 lines ($\lambda 1$ = 794.76 nm and $\lambda 2$ = 780.02 nm). (2:1260)

The same evaluation can be conducted for the ^{85}Rb atom to determine its optical wavelengths. As can be seen in Figure 2.11, one of the wavelengths for ^{85}Rb partially overlaps one of the wavelengths for ^{87}Rb. This close overlap at the higher wavelength provides a phenomenon in the operation of atomic clocks known as optical pumping. The term optical pumping refers to the redistribution of atoms among their fine or hyperfine-structure levels by means of light. As part of the design of rubidium clocks, a filter cell is usually found in between the absorption cell and the rubidium lamp. This filter cell is filled with ^{85}Rb atoms and an argon buffer gas. Because the D1 lines do not overlap totally for ^{85}Rb and ^{87}Rb, a buffer gas is used in the filter cell. This buffer gas (usually argon or nitrogen) under pressure can shift or broaden the ^{85}Rb lines to provide for a good overlap of the ^{87}Rb D1 line. (5:73)

Using argon as the buffer gas, the following approximate values for the ^{85}Rb shift and broadening parameters have been reported: A shift of -18 MHz/Torr for D1, -14 MHz/Torr for D2, and a broadening of approximately 10-20 MHz/Torr. (2:1260)

The resultant effect of overlapping the D2 lines is such that the ^{87}Rb visible light, as it passes through the filter cell, has the energy at the D1 wavelength absorbed by the now shifted ^{85}Rb D1 wavelength. As the light exits from the filter cell, it is composed mostly of the energy associated with the D2

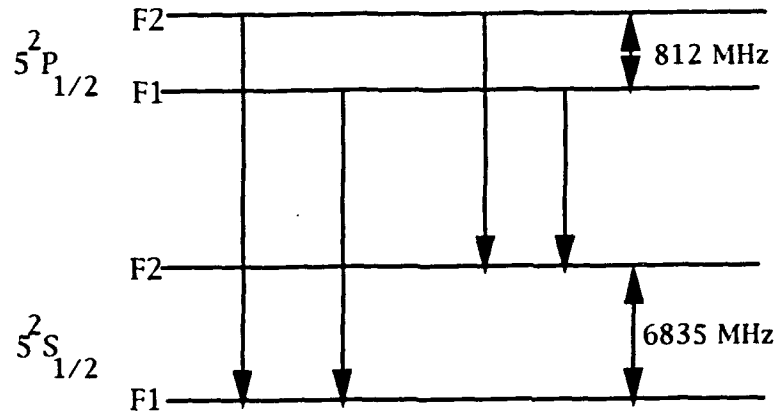

Figure 2.9 Zeeman Transitions Producing ^{87}Rb D2 Line

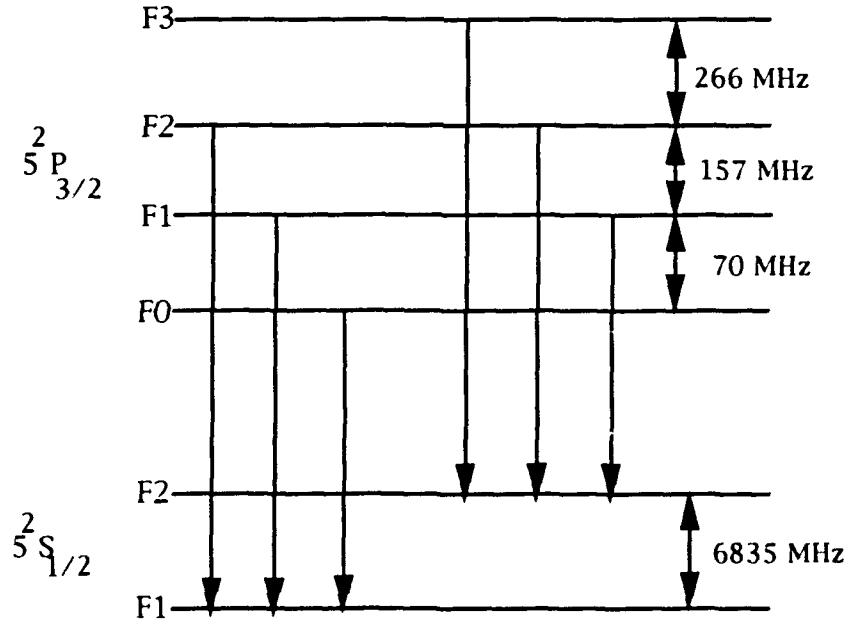

Figure 2.10 Zeeman Transitions Producing ^{87}Rb D1 Line

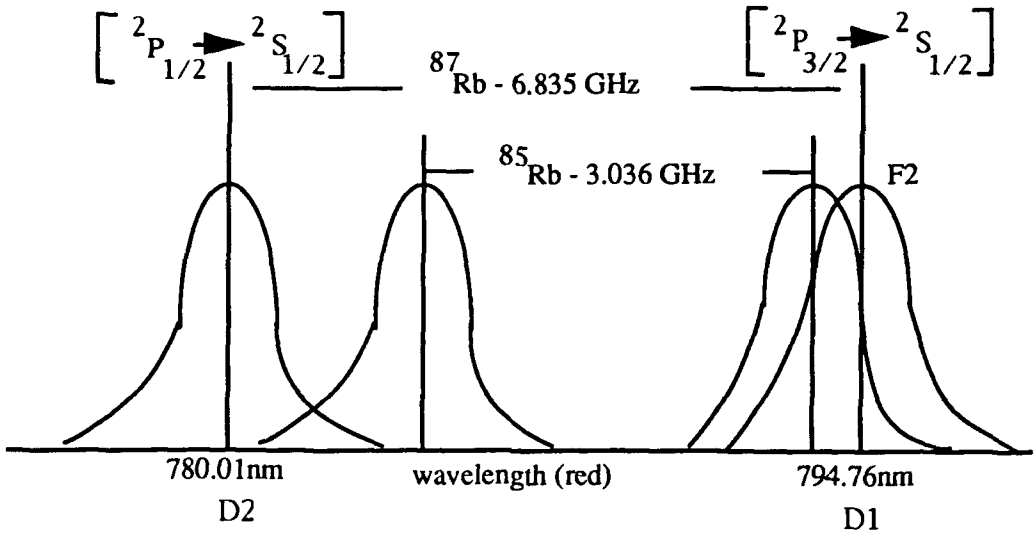

Figure 2.11 Rubidium Optical Emission

line. As it enters the absorption cell, which contains the ^{87}Rb atoms, the light is absorbed from only the one unfiltered wavelength line, D2. Thus, an imbalance in the fine or hyperfine-structure is achieved. (2:1262)

As can be seen in Figure 2.11, the primary resonance frequency is approximately 6.835 GHz for ^{87}Rb and approximately 3.036 GHz for ^{85}Rb. Both atomic structures can be used in the operation of a Rubidium atomic clock. However, because of its higher frequency, ^{87}Rb provides better timing resolution.

Rubidium Hyperfine Structure (2:1265-1268)

It was seen that in the presence of an external magnetic field the energy levels experience a Zeeman splitting effect. In the ground state ($^2S_{1/2}$), it has been seen that a splitting occurs into two sublevel ground states due to the

nuclear spin effect within the atomic magnetic field produced by the electron. These two states, named F1 and F2, were determined through Equations 2-32 and 2-33. The Zeeman splitting of each of these levels is due to subjecting the atomic structure to an external magnetic field. As the external magnetic field (B) increases, the distance between these hyperfine levels increase. An expanded representation of these hyperfine levels is seen in Figure 2.12. Following the state selection rule defined before, transitions between these hyperfine states can only occur between levels which differ by 0 or +/- 1.

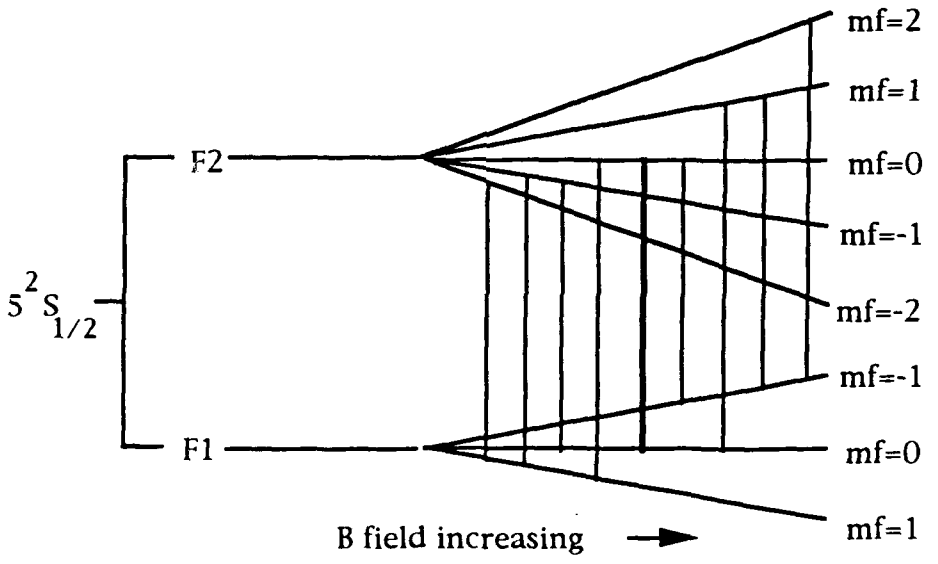

Figure 2.12 Hyperfine Splitting of ^{87}Rb Ground State

In reality, however, the Zeeman splitting does not occur linearly. As the B field increases to large values (>100 gauss), the hyperfine lines become non-linear. The regions used in rubidium clocks are linear, since the B fields are controlled under 1 Gauss. The bold line between the F2; m_f=0 and F1; m_f=0 states occur at a frequency equivalent to 6.835... MHz. These transitions are the ones used in the rubidium atomic clocks. A more accurate representation of these hyperfine energy levels is presented in the next section.

There are eight different possible transitions that can occur between the F1 and F2 ground states. However, there are two pairs of transitions that are equivalent in frequency on both sides of the F2 (m_f=0) to F1 (m_f=0) transition, which sum to produce a slightly stronger signal. So, exciting each of these transitions at the appropriate frequency and plotting these transition lines, only seven frequencies (also called the Zeeman frequencies) will be seen. These Zeeman frequencies are referred to as π or σ transitions based on the value of Δm_f. The π transitions refer to those frequencies associated with a Δmf=0, and σ transitions are those referring to a $\Delta m_f = \pm 1$. As the B-field is increased or decreased the frequency difference between the transitional frequencies will increase or decrease, respectively. The association of the value of transitional frequencies will be discussed in more detail in the next section.

An electromagnetic wave applied to the absorption cell, set at the identical frequency of the desired transition, will stimulate the electron to make the transition, whereby, the resonance frequency (in this case 6.835 GHz) is produced. This is the fundamental principle behind the operation of the atomic clock.

Rubidium Hyperfine Energy Levels

The theoretical energy level equation associated with the $^2S_{1/2}$; F1 and F2 hyperfine splitting can be calculated from the following equation (2:29):

$$E(F, m_f) = -[(\Delta W/4)\ (2I+1)] - [g_i\ \mu_B\ B_o\ m_f] \pm 1/2\ [(\Delta W/4)\ (2I+1)]\ [1 + (4m_f/2I+1)K + K^2]^{1/2} \qquad 2\text{-}34$$

where

$$\Delta W = 4/3\ [\ (m\ c^2\ \alpha^4\ g_i)/n^3)]\ [\ 1 + (m/\ Mp)\ ]^{-3} \qquad 2\text{-}35$$

and

$$K = [\ (g_j + g_i)\ \mu_B\ B_o\ ]\ /\ \Delta W\ (2I + 1)\ /\ 4] \qquad 2\text{-}36$$

Most of the constants for rubidium have been discussed in the previous sections, but will be repeated here for clarity (2:25):

m (electron mass) = 9.10910×10^{-28} g

Mp (proton mass) = 1.67252×10^{-24} g

g_i (Lande g factor for nuclear spin) = .000995141

g_j (Spectroscopic splitting factor) = 2.002331

m_B (Bohr magneton) = 9.2732×10^{-21} erg/gauss

c (speed of light) = 2.9917925×10^8 m/sec

α (fine structure splitting constant) = .00729720

I (nuclear spin magnetic moment) = 3/2

B_o = the applied magnetic field (variable)

With the exception of the variable B_0, the only other factor in the energy equation that is not a constant is m_f. As was seen in Figure 2.12, the F2 level has five m_f components, whereas, the F1 level has only three. The plus or minus factor in Equation 2.34 relates to the energy value calculations for the F2 and F1 hyperfine lines, respectively. A plot of the theoretical hyperfine energy states for ^{87}Rb is represented in Figure 2.13 for magnetic field values between 0 and 1 Gauss. These F2 and F1 hyperfine energy values have also been provided in Table 2.1 and Table 2.2, respectively.

Note that on Figure 2.13 an energy bias was removed from both F1 and F2 for plotting purposes, since the actual energy differentials are in the neighborhood of 10^{-21} ergs. For F1, subtract 2.83×10^{-17} ergs from plotted points for actual energy value, and for F2, add 1.7×10^{-17} ergs.

From the energy values listed in Tables 2.1 and 2.2, the theoretical value for the center frequency (υ_0) can be evaluated using the F2; m_f=0 to F1; m_f=0 transitions and applying Equation 2-8. Therefore, the theoretical value for ^{87}Rb (called υ_{HFS}) is calculated at 6.83468261(43) GHz (2:24). The parenthesis indicates the uncertainty digits based on the number of significant digits available for the constants.

As Figure 2.13 indicates, the energy values for both the F2 and F1 states at the lower magnetic fields appear to be linear. Again, the non-linearity occurs at much higher B field values. This non-linearity can be seen in Figure 2.14, as the magnetic field is increased to 4500 Gauss.

Since the investigation in this study will only be concerned with the linear regions of the hyperfine splitting, there exists a linear relationship between all the Zeeman transitions. Historically, rubidium clock frequency analysis uses just one of the six possible Zeeman transitions (excluding the

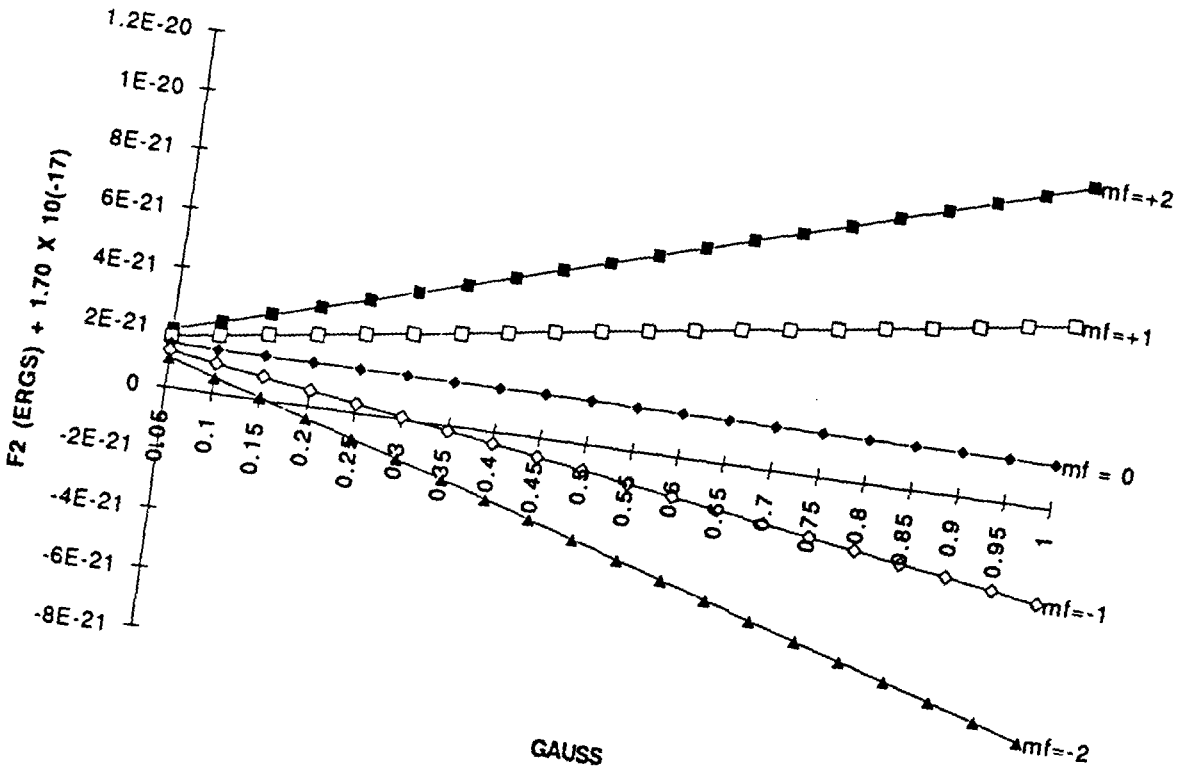

Figure 2.13 Plot of ^{87}Rb F1 and F2 Hyperfine Energy Values for Coil Magnetic Field Levels From 0 to 1 Gauss

Table 2.1 ^{87}Rb F2 Hyperfine Energy Values
for Coil Magnetic Field Levels From 0 to 1 Gauss

Gauss	10^{-17} Ergs				
B-FIELD	mf=+2	mf=+1	mf=0	mf=-1	mf=-2
0.05	1.69819159	1.69816842	1.69814524	1.69812207	1.69809889
0.1	1.69823794	1.69819159	1.69814524	1.69809889	1.69805254
0.15	1.69828429	1.69821477	1.69814525	1.69807572	1.69800619
0.2	1.69833065	1.69823795	1.69814525	1.69805255	1.69795984
0.25	1.698377	1.69826113	1.69814525	1.69802937	1.69791349
0.3	1.69842335	1.69828431	1.69814526	1.6980062	1.69786714
0.35	1.6984697	1.69830749	1.69814527	1.69798303	1.69782079
0.4	1.69851605	1.69833067	1.69814527	1.69795986	1.69777444
0.45	1.6985624	1.69835385	1.69814528	1.69793669	1.69772808
0.5	1.69860875	1.69837703	1.69814529	1.69791352	1.69768173
0.55	1.6986551	1.69840021	1.6981453	1.69789036	1.69763538
0.6	1.69870145	1.6984234	1.69814531	1.69786719	1.69758903
0.65	1.6987478	1.69844658	1.69814532	1.69784402	1.69754268
0.7	1.69879415	1.69846977	1.69814534	1.69782086	1.69749633
0.75	1.6988405	1.69849295	1.69814535	1.69779769	1.69744998
0.8	1.69888686	1.69851614	1.69814536	1.69777453	1.69740363
0.85	1.69893321	1.69853933	1.69814538	1.69775136	1.69735728
0.9	1.69897956	1.69856252	1.6981454	1.6977282	1.69731093
0.95	1.69902591	1.6985857	1.69814541	1.69770504	1.69726458
1	1.69907226	1.69860889	1.69814543	1.69768188	1.69721823

Table 2.2 ^{87}Rb F1 Hyperfine Energy Values
for Coil Magnetic Field Levels From 0 to 1 Gauss

Gauss	10^{-17} Ergs		
B-FIELD	mf=-1	mf=0	mf=+1
0.05	-2.8302188	-2.83024207	-2.83026534
0.1	-2.83019554	-2.83024207	-2.83028861
0.15	-2.83017227	-2.83024207	-2.83031188
0.2	-2.830149	-2.83024208	-2.83033515
0.25	-2.83012574	-2.83024208	-2.83035842
0.3	-2.83010248	-2.83024209	-2.83038169
0.35	-2.83007921	-2.83024209	-2.83040496
0.4	-2.83005595	-2.8302421	-2.83042823
0.45	-2.83003269	-2.83024211	-2.83045151
0.5	-2.83000943	-2.83024212	-2.83047478
0.55	-2.82998617	-2.83024213	-2.83049806
0.6	-2.82996291	-2.83024214	-2.83052133
0.65	-2.82993965	-2.83024215	-2.83054461
0.7	-2.82991639	-2.83024216	-2.83056789
0.75	-2.82989313	-2.83024218	-2.83059117
0.8	-2.82986988	-2.83024219	-2.83061444
0.85	-2.82984662	-2.83024221	-2.83063772
0.9	-2.82982337	-2.83024222	-2.830661
0.95	-2.82980011	-2.83024224	-2.83068429
1	-2.82977686	-2.83024226	-2.83070757

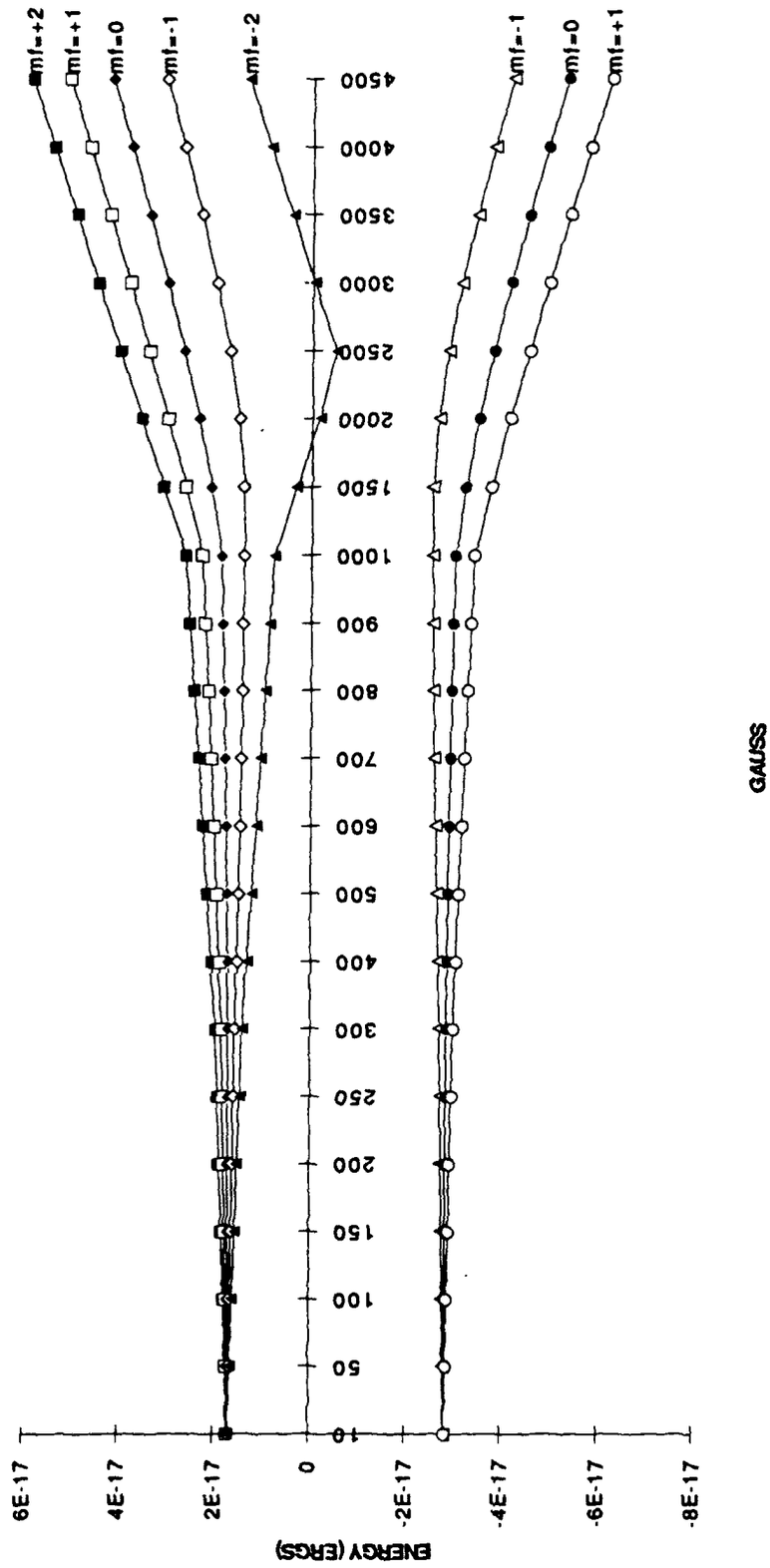

Figure 2.14 Plot of Theoretical ^{87}Rb F2 and F1 Hyperfine Energy Values for Large Magnetic Fields

center frequency), and is referred to as the primary Zeeman. This primary Zeeman frequency (υ_z), is determined from the the F2; m_f=-1 to F1; m_f=-1 (Δmf=0) transition. The actual value of the frequency is not used, but is represented as the difference from the primary center resonance frequency υ_0. Theoretically, there is a linear relationship between these two frequencies (at low B field settings) that can be calculated. The only variable that exists now from Equation 2-34 is the magnetic field value (B_0), since the transition level (m_f = -1) for this primary Zeeman frequency (υ_z) has now been defined.

A similar theoretical relationship can be made for the determination of the center resonance frequency (υ_0) which also depends on the value of the magnetic field. As υ_0 is determined by the F2; mf=0 to F1; mf=0 hyperfine transitions, then a closer look at Equation 2-34 will allow for certain terms to go to zero, since mf=0. A remaining term will be the K term established in Equation 2-36. Since B_0 is contained in the evaluation of the term K, and the remainder of the terms are constants, then υ_0 can also be represented in a more simplified manner as can the primary Zeeman frequency. This leads to a simplified theoretical expression for both the center and primary Zeeman frequencies:

$$\upsilon_0 = \upsilon_{HFS} + K_0 B_0^2 \qquad 2\text{-}37$$

and

$$\upsilon_z = K_z B_0 \qquad 2\text{-}38$$

where K_0 is 1401940 Hz/Gauss and K_z is 575.14 Hz/Gauss.

Both of these observations can be seen in Figures 2.15 and 2.16, which plots υ_0 and υ_z, respectively, relative to varying the magnetic field between 0 and 1 Gauss. The data for these plots are represented in Table 2.3, which applies the energy values from each of the hyperfine lines indicated in Table 2.1 and Table 2.2 to the frequency calculation from Equation 2-8. The frequency associated with each allowable energy transition is supplied, but the individual transitions of interest are those for the center frequency υ_0 (F2; mf=0 to F1; mf=0 transition) and the frequency (F2= mf=-1 to F1; mf=-1 transition) which is used to determine the primary Zeeman frequency υ_z. The value of υ_z is also provided in Table 2.3, which has incorporated the frequency difference calculation from υ_0 as discussed above.

Helmholtz Coil and B-Field Theory

The absorption cell B-field used in the RFS-10 design is a Helmholtz coil. A representative view of the coil configuration used in the RFS-10 rubidium clock can be seen in Figure 2.17. This configuration consists basically of two circular electrical coils of the same radius, a common axis, and separated by some arbitrary distance (depending on desired results). The use of the Helmholtz has played an important role in scientific design since it can produce a relatively uniform magnetic field over a small region of space. The determination of the B-field can be accomplished by knowing the dimensions of the coil, the number of turns (N) in each of the circular coils, and the current (I) applied to each of the coils.

The magnetic induction at any point along the Z axis (boresight) of the

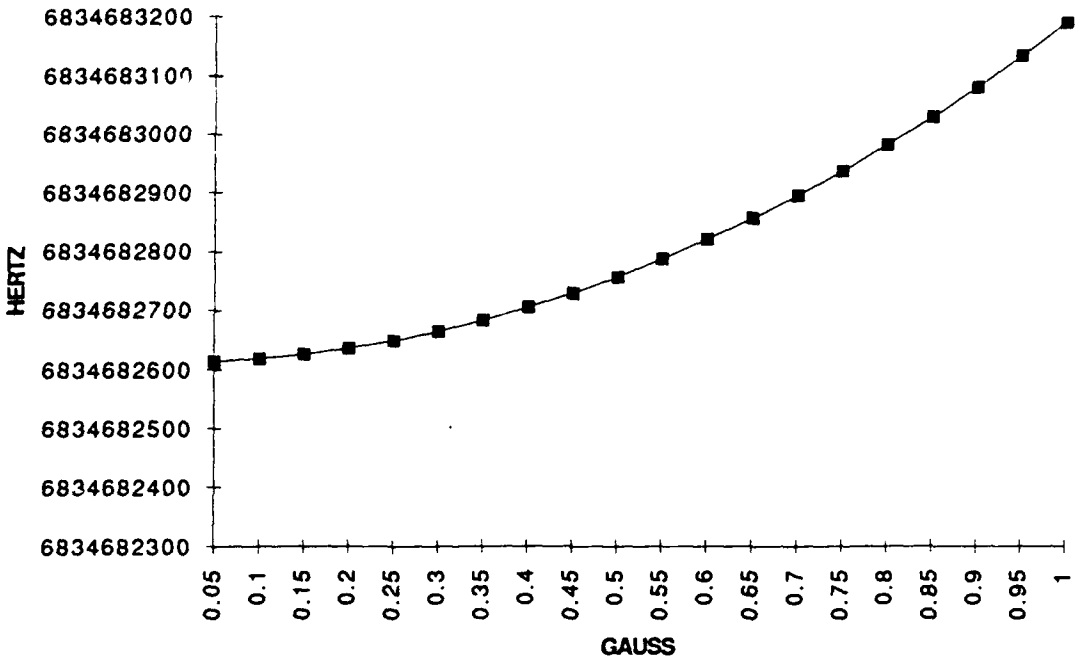

Figure 2.14 ^{87}Rb Center Frequency Value as a Function of Varying Magnetic Field From 0 to 1 Gauss

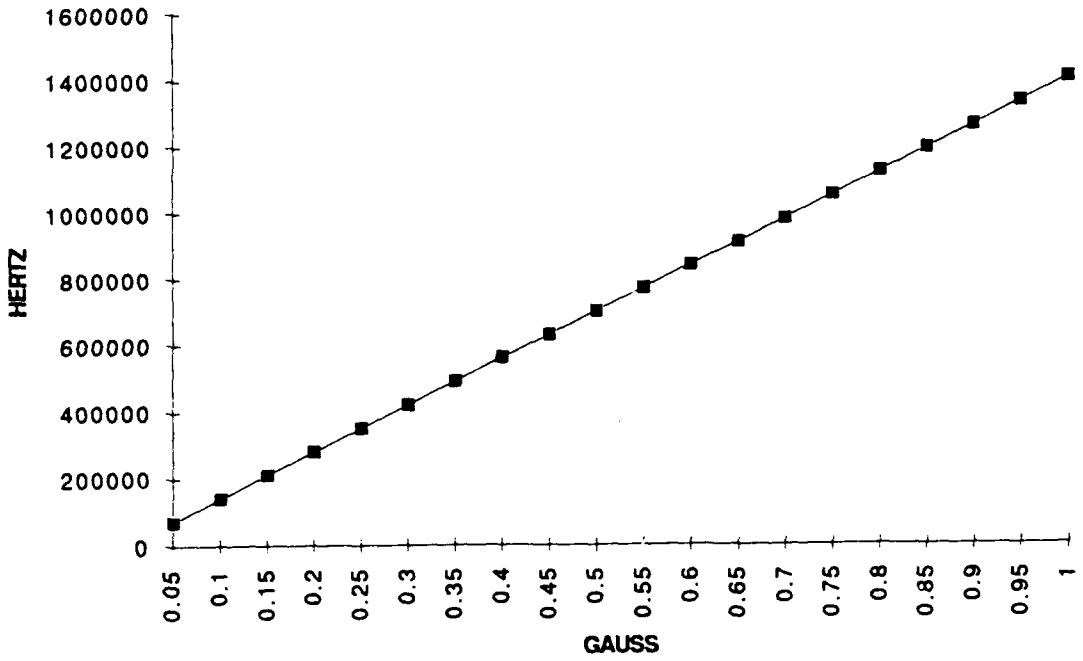

Figure 2.15 ^{87}Rb Primary Zeeman Frequency Value as a Function of Varying Magnetic Field From 0 to 1 Gauss

Table 2.3 Theoretical Frequency Values for All Allowable Hyperfine Energy Transitions for ^{87}Rb in a Magnetic Field from 0 to 1 Gauss

Frequency (Hz)

GAUSS	F2-F1	F2-F1	F2-F1	F2-F1	F2-F1	F2-F1	F2-F1	F2-F1	F2-F1	vo-vz
B-FIELD	mf=0-mf=0	mf=2-mf=1	mf=1-mf=0	mf=1-mf=1	mf=0-mf=1	mf=0-mf=-1	mf=-1-mf=-1	mf=-1-mf=0	mf=-2-mf=-1	
0.05	6834682614	6834787688	6834717593	6834752710	6834717732	6834647496	6834612518	6834647636	6834577538	70096.8131
0.1	6834682619	6834892765	6834752575	6834822810	6834752854	6834612382	6834542424	6834612661	6834472465	140194.345
0.15	6834682626	6834997843	6834787560	6834892912	6834787978	6834577271	6834472333	6834577686	6834367393	210292.598
0.2	6834682636	6835102922	6834822547	6834963016	6834823104	6834542162	6834402244	6834542719	6834262321	280391.565
0.25	6834682649	6835208002	6834857537	6835033122	6834858234	6834507055	6834332158	6834507751	6834157251	350491.253
0.3	6834682665	6835313083	6834892530	6835103230	6834893365	6834471951	6834282073	6834472787	6834052182	420591.66
0.35	6834682683	6835418165	6834927525	6835173341	6834928500	6834436849	6834191991	6834437824	6833947114	490692.785
0.4	6834682705	6835523248	6834962522	6835243454	6834963636	6834401750	6834121910	6834402865	6833842047	560794.628
0.45	6834682729	6835628332	6834997522	6835313588	6834998776	6834366654	6834051832	6834367908	6833736981	630897.19
0.5	6834682757	6835733417	6835032525	6835383685	6835033917	6834331560	6833981756	6834332953	6833631916	701000.471
0.55	6834682787	6835838504	6835067530	6835453804	6835069062	6834296469	6833911682	6834298001	6833526853	771104.469
0.6	6834682820	6835943591	6835102537	6835523926	6835104208	6834261380	6833841611	6834263051	6833421790	841209.186
0.65	6834682856	6836048680	6835137547	6835594049	6835139358	6834226293	6833771541	6834228104	6833316729	911314.621
0.7	6834682895	6836153769	6835172560	6835664175	6835174510	6834191209	6833701474	6834193159	6833211668	981420.773
0.75	6834682936	6836258860	6835207575	6835734302	6835209664	6834156128	6833631409	6834158217	6833106609	1051527.64
0.8	6834682981	6836363952	6835242592	6835804432	6835244821	6834121049	6833561346	6834123278	6833001550	1121635.23
0.85	6834683028	6836469044	6835277612	6835874564	6835279980	6834085973	6833491285	6834088347	6832896493	1191743.54
0.9	6834683079	6836574138	6835312635	6835944698	6835315142	6834050899	6833421226	6834053406	6832791437	1261852.56
0.95	6834683132	6836679233	6835347660	6836014835	6835350306	6834015828	6833351170	6834018474	6832686382	1331962.31
1	6834683188	6836784329	6835382688	6836084973	6835385473	6833980759	6833281115	6833983544	6832581328	1402072.77

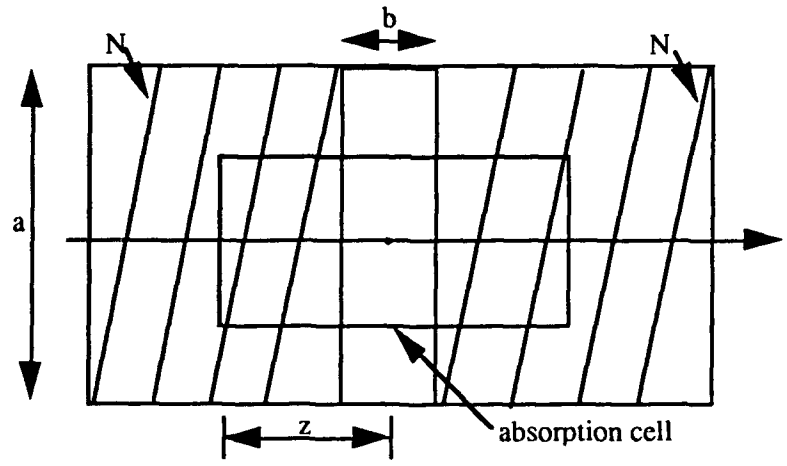

Figure 2.17 Cross Sectional View of RFS-10 Helmholtz Coil

coil can be evaluated from the following equation (16:154):

$$Bz(z) = (N \mu_o I a^2/2) \{ [1/ (z^2 + a^2)^{3/2}] + [1 / ((b-z)^2 + a^2)^{3/2}] \} \quad 2\text{-}39$$

where

N = 42 turns

μ_o = 1.2566371 x 10^{-6} H/m

z = 1.3208 cm

a = 1.53671 cm

b = .381 cm

I = variable current

A theoretical value for the B field within the Helmholtz coil can be seen graphically in Figure 2.18. The current value (I) for this plot was selected at 4.5

milli-amps. The average B field within the absorption cell was calculated using a least squares fit to the actual data (4:496).

There are still some non-uniform aspects to the Helmholtz coil. A least squares fit was applied to the curve to determine the average value of B_0 throughout the absorption cell. This average is the value of B_0 during applications of Equations 2-31 through 2-34. The value of B_0 was plotted in Figure 2.17 using only one current (I) value, but the shape of this curve is consistent with all others.

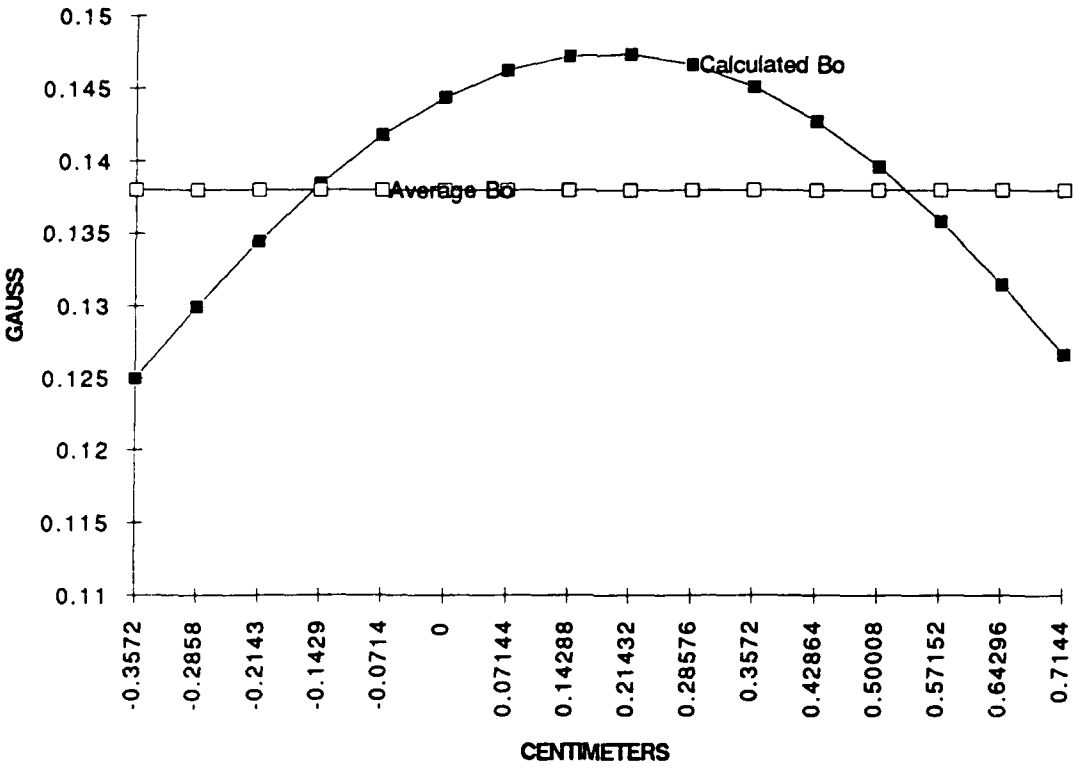

Figure 2.17 Calculated Magnetic Field (B_0) for the Rubidium Model RFS-10 Internal Helmholtz Coil at a Current of 4.5 Milliamps

III. *Experimental Procedure*

Measurement System

The C-field experiment was performed in a laboratory on the commercial double-cell Rb frequency standard, EG&G Model RFS-10. This standard was modified to allow access to the C-field coil wires and the microwave power source. Figure 3.1 is a block diagram of the measurement system. Both of the parameters that are varied, namely the C-field current and the microwave power, are computer controlled; the current is set by a precision constant-current generator, while the microwave power is changed by using an electronic switch to change the resistance of a bias resistor on the step-recovery diode. The bias resistors were chosen to change the microwave power by +1.3, -1.1, -2.2, and -4.0 dB with reference to the nominal, factory-set power level P_0. The 6.835-GHz microwave power to the cell was sampled by coupling with a two-turn coil on the 6.835-GHz coaxial signal line. The bias resistors were chosen by using a Hewlett-Packard (H-P) model 8566 spectrum analyzer to observe the change in microwave power on this coupled signal.

The entire measurement system is controlled by an H-P series 300 computer, which also acquires and processes the data. Figure 3.2 is a block diagram of the frequency measurement system. The frequency reference for both the Fluke synthesizer and the H-P counter is an H-P model 5061A-004 Cesium (Cs) frequency standard.

This procedure was accomplished following calibration and specification steps identified by the manufacturer. Steps were carefully taken to ensure no damage would occur to the test article and the test set-up

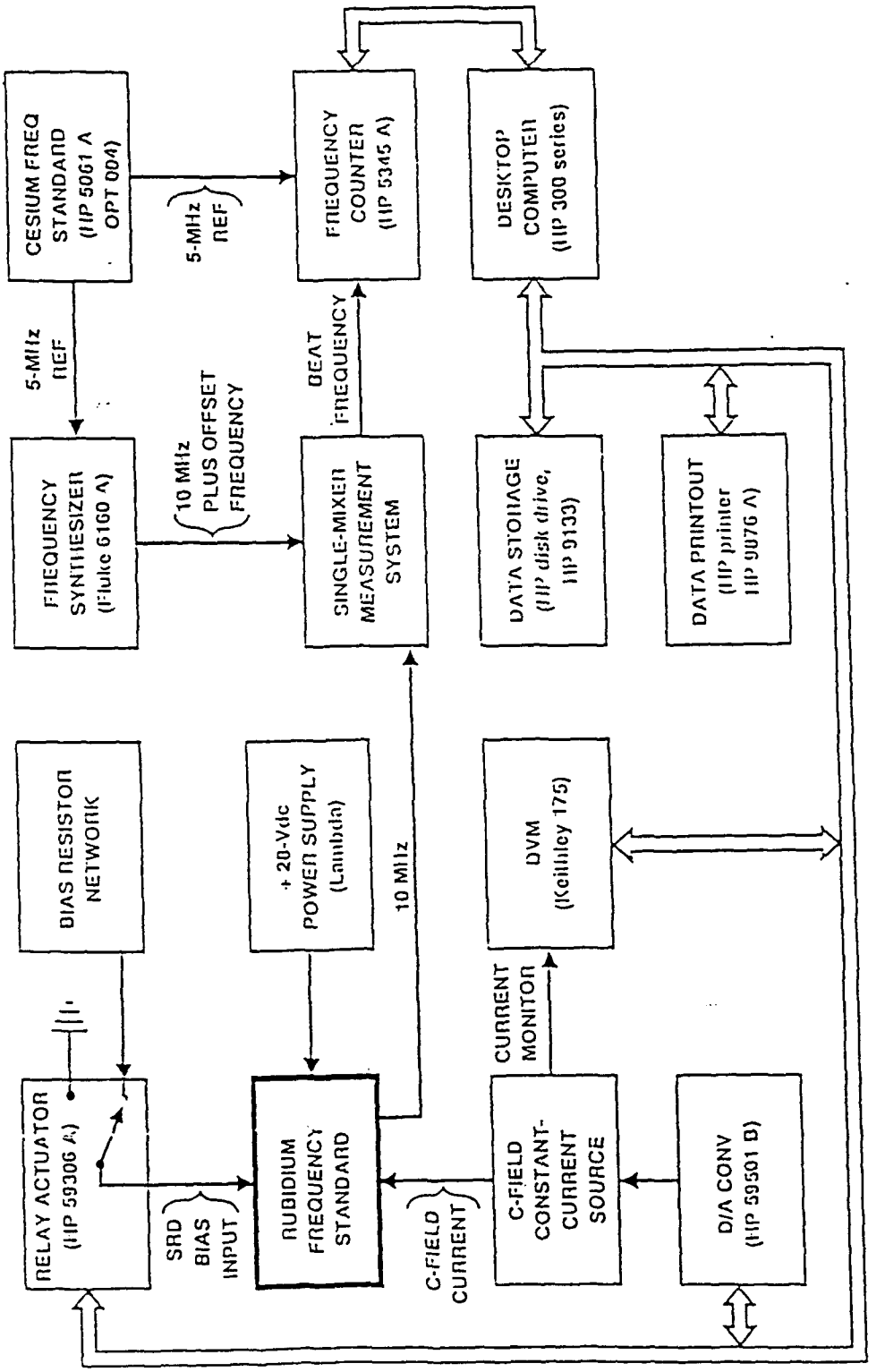

Figure 3.1 Measurement System Block Diagram

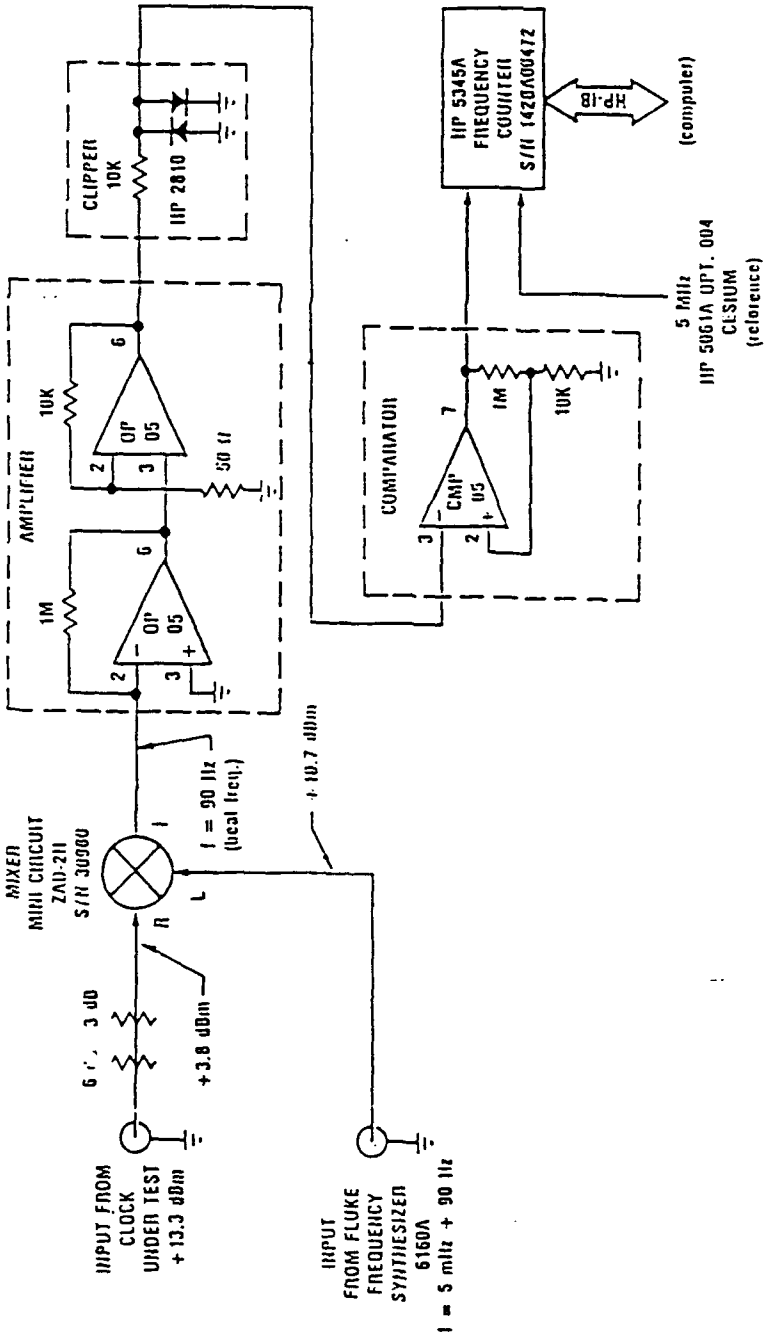

Figure 3.2 Frequency Measurement Block Diagram (24:18)

equipment. After confident in the proper operation of all the equipment, the following steps were taken in sequence to conduct the experiment.

1. Set the C-field current at some low value (typically 2 to 6 mA) and the microwave power at some value (e.g. at the nominal value P_0).

2. Measure the beat frequency over some long averaging time T (typically 500-1000 sec).

3. Change the microwave power level [e.g. to (P_0 - 1.1 dB)].

4. Measure the beat frequency over T again.

5. Increase the C-field current by some predetermined amount (typically 0.5 mA).

6. Measure the beat frequency over T again.

7. Change the microwave power back to the initial value.

8. Repeat steps 2 through 7 until the final C-field current (typically 14 to 20 mA) is reached.

To determine the functional relationship between the C-field current and the Zeeman frequency, the microwave frequency is swept over approximately 1 MHz, centered about the main Rb resonance line. The output of the standard's dc-coupled current-to-voltage converter is then plotted as a function of frequency. Figure 3.3, for a C-field current of 4.5 milli-amps, is a typical plot. This plot shows the main Rb transition state, as well as the four σ transitions and the two π transitions (the π transitions are used to define the Zeeman frequency υ_z). It should be noted that the 0-to-39.53-mV ordinate in Figure 3.3 rides on top of a 5 Volt bias, which is filtered out with a precision low-noise floating voltage source. The Zeeman frequency is read from the plot in Figure 3.3. The measurement is then repeated for different B-field currents.

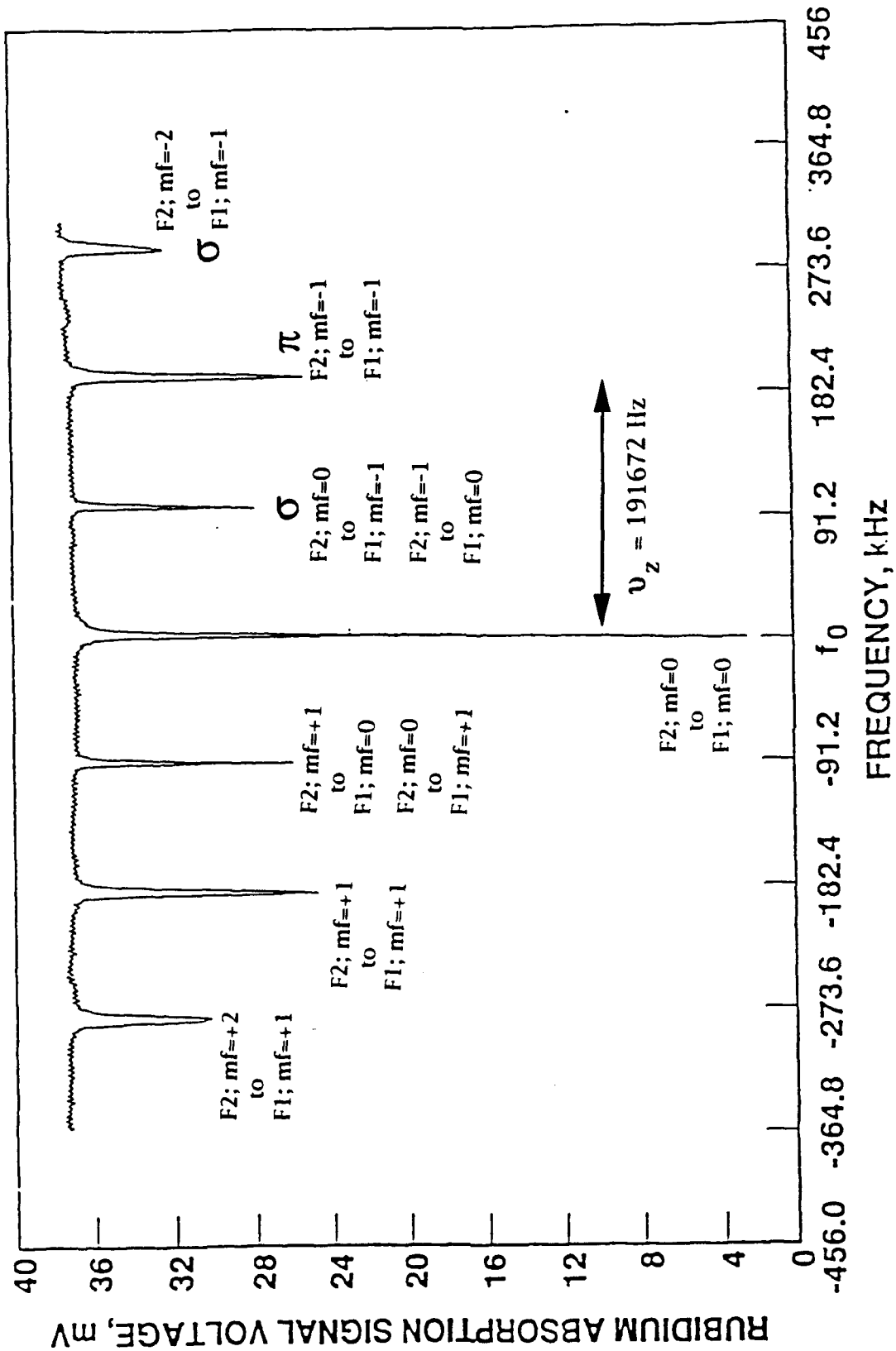

Figure 3.3 Zeeman Frequency Plot for RFS-10 Rubidium Clock at Nominal Factory Setting

Measurement Results

Figure 3.4 shows the summary of results of measurements made on the commercial Rb standard for changes in the microwave power level of +1.3, -1.1, -2.2, and -4.0 dB. Each data point, which represents the difference between two 1000-sec averages, is calculated as the difference in output frequency between the frequency at the higher power and that at the lower power, both powers being normalized to the nominal output. In other words,

$$y = (\upsilon_h - \upsilon_l) / 10 \text{ Mhz} \qquad 3\text{-}1$$

where υ_h is the average output frequency for the higher microwave power and υ_l is the average output frequency for the lower microwave power. From Figure 3.4 we see that the maximum frequency change for the +1.3 and -1.1 dB data is about 3×10^{-11}, that for the -2.2 dB data is about 6×10^{-11}, and that for the -4.0 dB data is about 1.4×10^{-10}. As a function of the change in microwave power, the maximum frequency change is about 2.6×10^{-11}/dB.

The three curves have a similar shape, namely one that is fairly flat for Zeeman frequencies between 100 and 300 kHz, then decreasing monotonically for Zeeman frequencies between 300 and 850 kHz. In separate tests, data was obtained for the region of low Zeeman frequency. Figure 3.5 shows the results of those tests for the same microwave power changes as in Figure 3.4. From the curves in Figure 3.5, it is seen that there are zero crossings (indicating no frequency shift) at about 13 and 37 kHz. The operation of the clock at one of these points would result in zero sensitivity

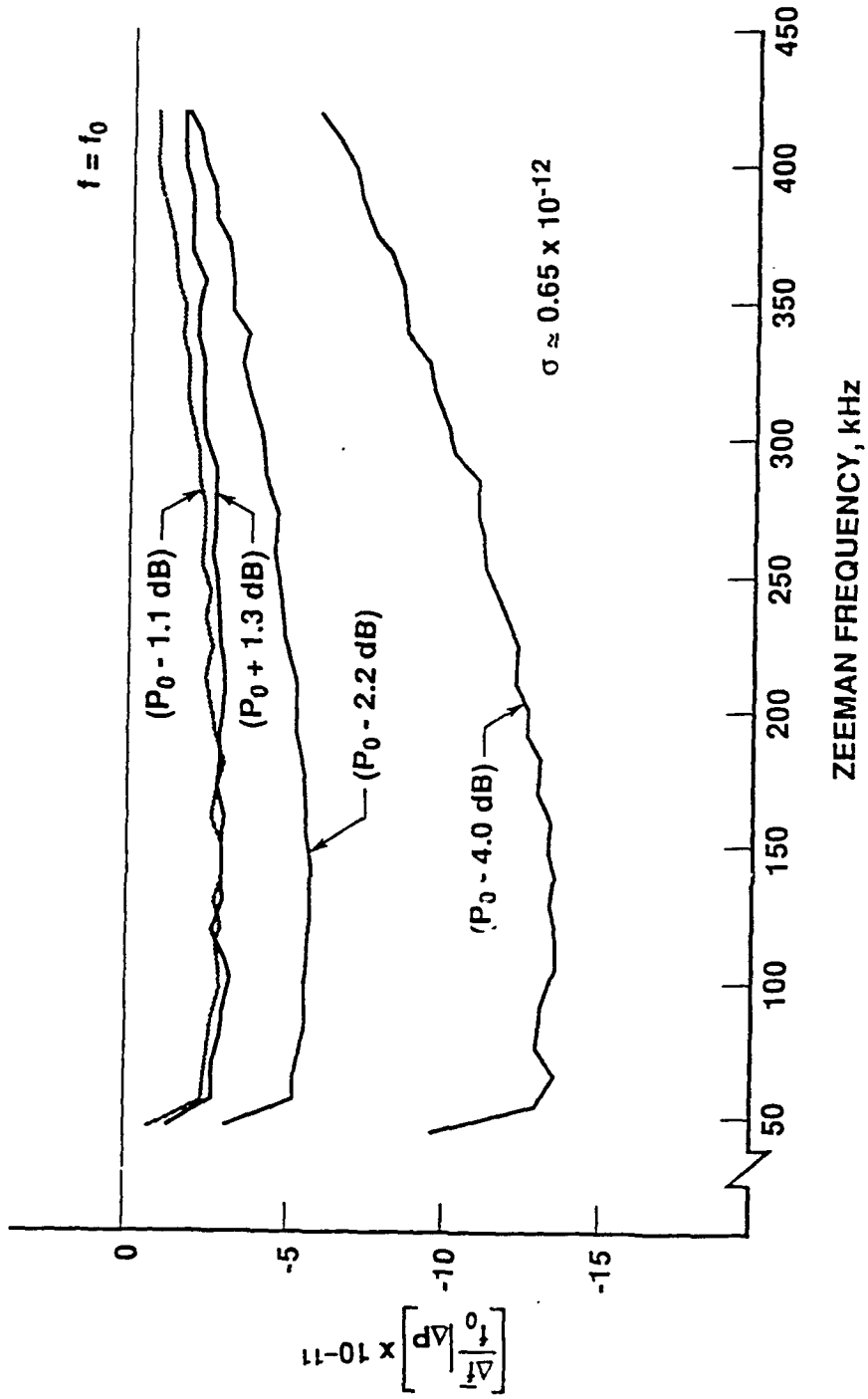

Figure 3.4 Fractional Frequency Changes as a Function of B-Field for Microwave Changes of +1.3, -1.1, -2.2, and -4.0 dB

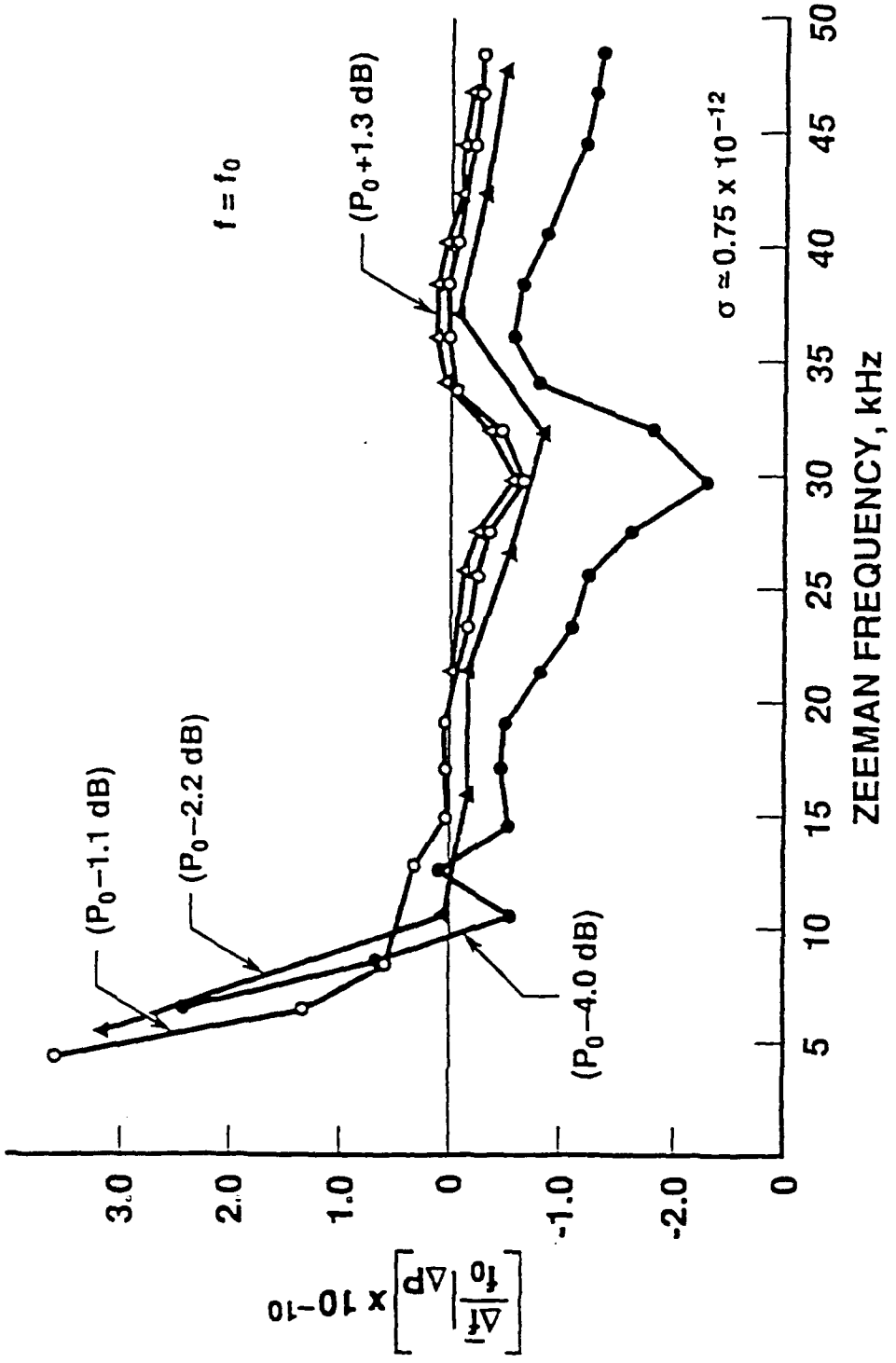

Figure 3.5 Fractional Frequency Changes as a Function of Small B-Field for Microwave Changes of +1.3, -1.1, -2.2, and -4.0 dB

of the clock frequency to microwave power changes and may result in improved long-term clock stability, as had been observed by De Marchi in his investigations of cesium frequency standards (12:57). The manufacturer's B-field current setting for this clock was 4.5 mA, which gave the primary Zeeman frequency of approximately 191 kHz. Operating the clock at lower B-fields would also have the advantage of decreasing clock sensitivity to B-field current; i.e., a change in B-field current results in a smaller change in output frequency when the B-field current is small.

A plot of the rubidium clock center frequency span measured at the nominal factory magnetic field setting (4.5 mA) and nominal microwave power setting (P_0) is represented in Figure 3.6. The center frequency value (υ_0) in addition to the frequency span at the half power point is indicated on the plot. The cell lamp output voltage indicated on the y axis of the plot refers to a relative voltage change from the nominal operating output signal. This data rides on 1.2 Volt cell lamp output voltage, which has been subtracted for the purposes of plotting these relatively small (milli-volt) signal changes. The same data was collected for different microwave power points which include: P_0- 1dB, P_0- 3dB, P_0- 4dB, P_0+ 1dB, P_0+ 2dB, and P_0+ 3dB. The results of these measurements are indicated in Table 3.1. Using the data from this table, plot of the half-power linewidth frequency as a function of microwave cavity power measured from the nominal P_0 is represented in Figure 3.7. Also, Figure 3.8 plots the relative difference in center frequency (υ_0) measured against the same values of microwave power. There is an obvious large shift in both half-power frequency width and center frequency when the power is reduced below - 3dB. Between $\pm$ 3dB, the half-power linewidth frequency remains fairly constant at about 2 kHz, and the

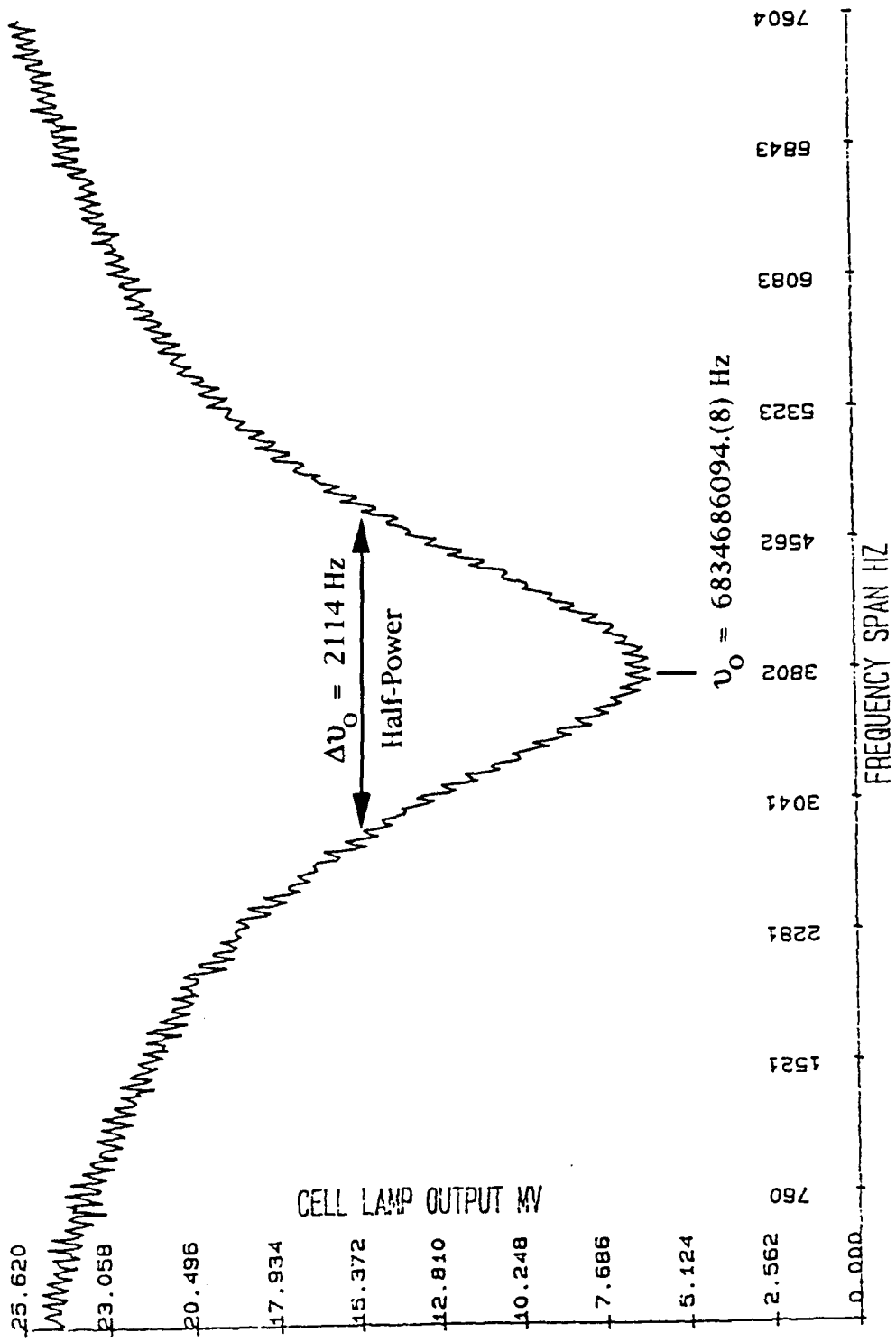

Figure 3.6 Center Frequency (υ_o) Line Width Plot for RFS-10 Rubidium Clock Measured at Nominal Factory Power Setting (P_o)

Table 3.1 Center Frequency (υ_0) and Half-Power Linewidth Frequency Measurements for Different Microwave Power Values

CAVITY POWER	HALF POWER SIGNAL STRENGTH	HALF-POWER FREQUENCY WIDTH	CENTER FREQUENCY
+ 3 dB	2.385 mV	2112.(5) Hz	6834686187.(9) Hz
+ 2 dB	2.575 mV	2191.(1) Hz	6834686141.(3) Hz
+ 1 dB	2.445 mV	2158.(6) Hz	6834686171.(6) Hz
P_0	2.350 mV	2114.(2) Hz	6834686094.(8) Hz
- 1 dB	2.185 mV	1915.(5) Hz	6834686187.(1) Hz
- 3 dB	1.640 mV	1580.(4) Hz	6834686186.(2) Hz
- 4 dB	0.215 mV	6261.(3)Hz	6834686020.(5) Hz

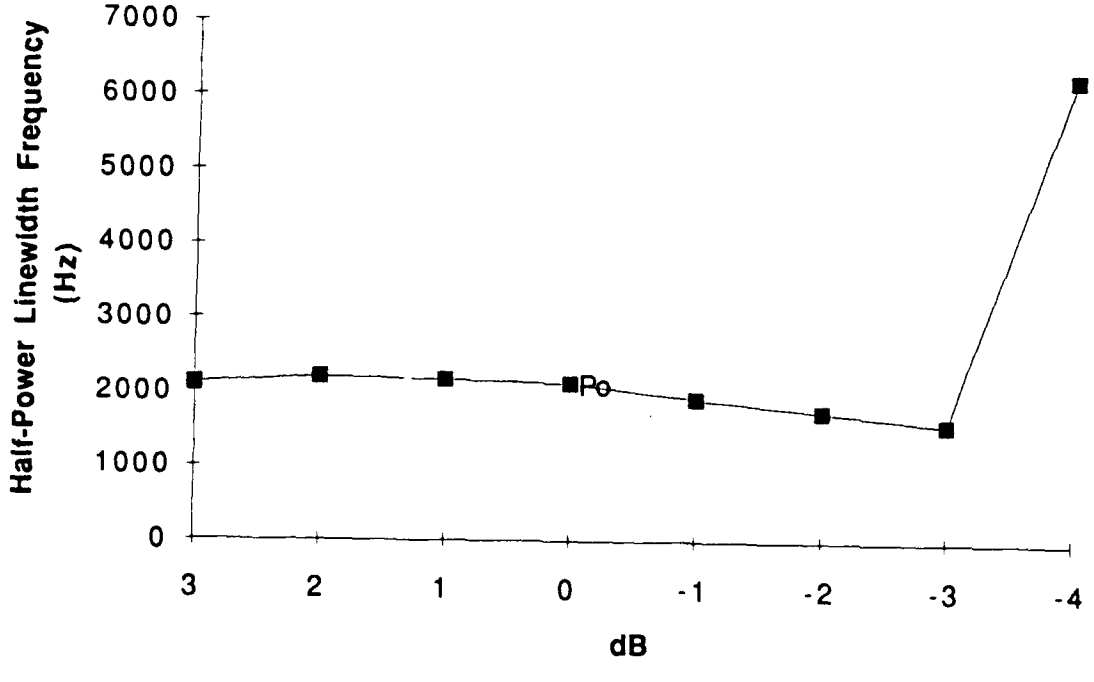

Figure 3.7 Measured Rubidium RFS-10 Half-Power Linewidth Frequency as a *Function of* Changing Microwave Power

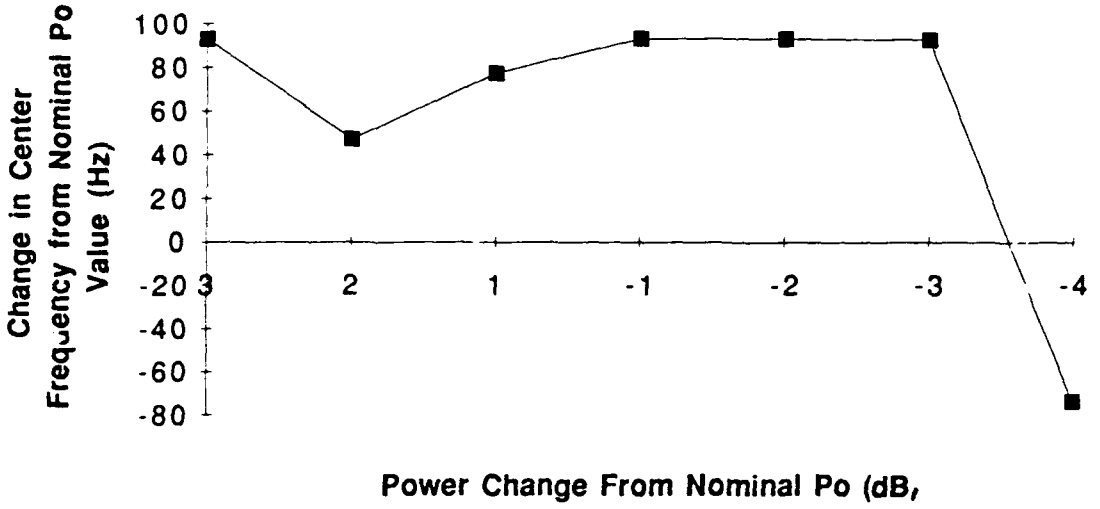

Figure 3.8 Measured Rubidium RFS-10 Center Frequency Differences as a Function of Changing Microwave Power

center frequency shift is always in the positive direction at about 90 Hz.

Sweeping the microwave power from lowest to highest possible values allowed on the clock adjustment, measurements of the lamp output signal voltages were taken and plotted in Figure 3.9. The selected power points discussed above are annotated on the plot to provide for a point of reference. The y-axis of the plot provides for a relative vice absolute change in lamp signal voltage as compared to the value observed from the nominal factory setting.

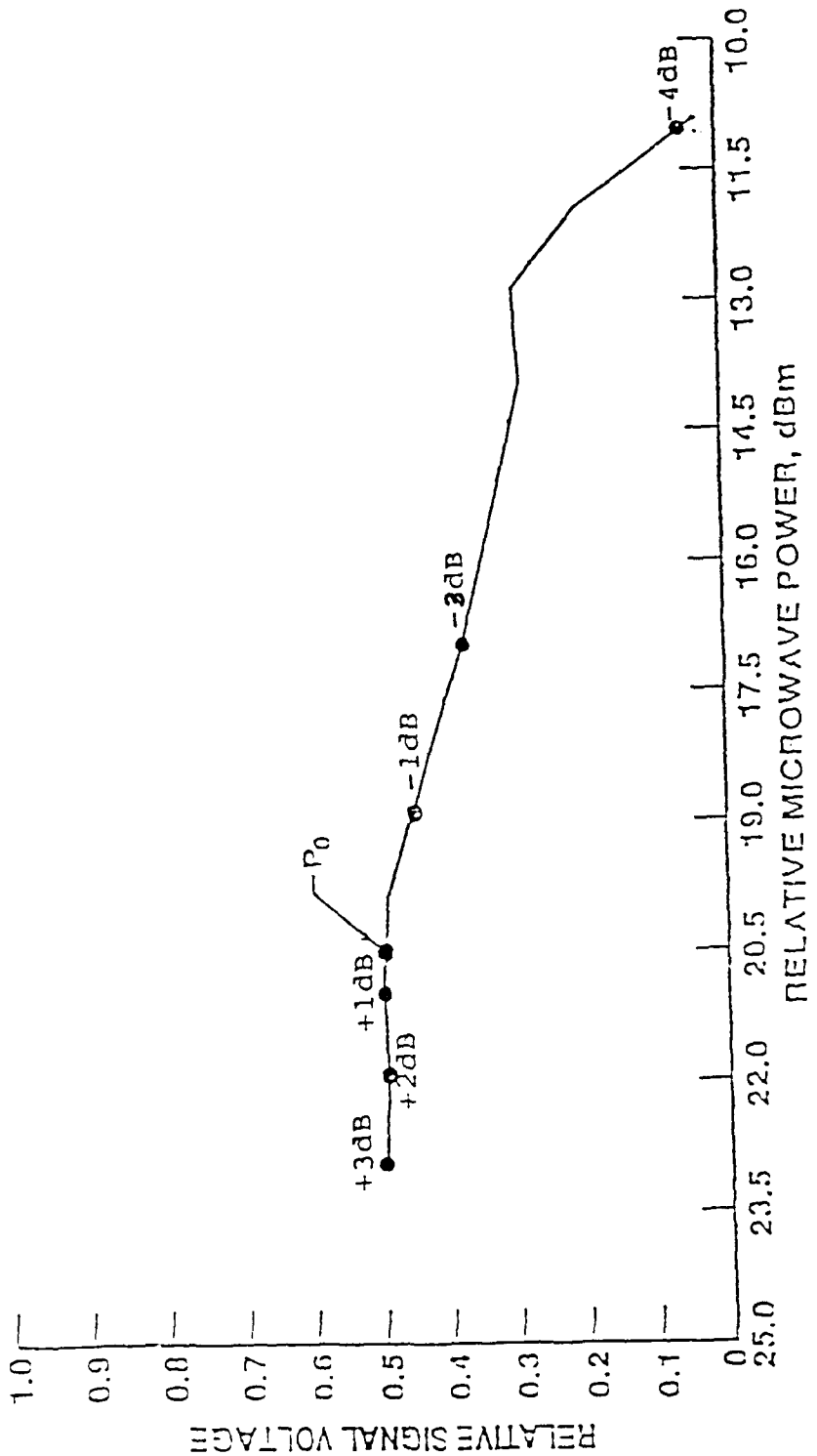

Figure 3.9 Measured Center Frequency (υ_o) Output Signal Voltage as a Function of Changing Microwave Power

IV. Analysis of Results

Hyperfine Theory Versus Experimental Results

Evaluation of the theoretical model of the ^{87}Rb hyperfine transition frequencies compared to the measured values obtained during this study requires an accurate measurement or calculation of the clock's coil magnetic field. As discussed in Chapter 2 (pages 2-27 through 2-33), the theoretical model for determining both the rubidium center frequency (υ_0) and primary Zeeman frequency (υ_z) rely on the knowledge of the magnetic field (B_0). Since measurement data can only be obtained from recording the magnetic field current, then alternate methods are required to determine an accurate magnetic field value. Using the Helmholtz coil model to calculate the magnetic field would not be appropriate since this model has not yet been validated through a theoretical comparison. However, determining the magnetic field through the use of Equations 2-34 through 2-38 will establish a theoretical baseline to compare measurement results against.

One set of measured values for magnetic field current, center frequency and primary Zeeman frequency are provided below which were used during this analysis, however, other measured values could have also been used to obtain the same results.

Coil current, $I = 4.50(0)\ mA\ (\pm\ 0.005)$

Zeeman Frequency, $\upsilon_z = 191672.(0)$ Hz ($\pm$ 0.1 Hz)

Center Frequency, $\upsilon_0 = 6834686094.(8)$ Hz ($\pm$ 0.1 Hz)

The above Zeeman frequency is applied to Equation 2-38 resulting in:

$$B_0(t) \approx 0.136719(1) \text{ Gauss}$$

(where (t) indicates theoretical). The last digit in parentheses indicates the precision uncertainty term based on the accuracy of the Zeeman frequency used ($\pm$ 0.1 Hz).

Applying the center frequency measurement identified above to Equation 2-37 provides the following magnetic field calculation (υ_{HFS} = 6.83468261(43) GHz - reference page 2.28):

$$B_0(t) = 0.049836(7) \text{ Gauss}$$

There is approximately a factor of 3 difference between these two calculations. Since the first calculation of the magnetic field above is independent of the center frequency (from Equation 2-38), then using the theoretical energy equation (2-34) should help in determining the most accurate value for the magnetic field. Referencing the data in Tables 2-1 through 2.3 and using the value of $B_0 \approx 0.136719(1)$ Gauss from above, a theoretical value for the primary Zeeman frequency can be obtained. This Zeeman is determined through the F2; mf=-1 to F1; mf=-1 energy transition. The results are as follows:

$$\upsilon_z(t) = 191673.(16) \text{ Hz}$$

There is approximately a 1 Hz difference between this calculated value and that which was measured. This good comparison indicates that this value of the magnetic field is accurate to determine the validation of the Helmholtz coil model.

Also using the theoretical energy equation (2-34) and Tables 2-1 through 2-3, a value for the center frequency can be calculated using the F2; mf =0 to F1; mf=0 transition. Again the same value (0.139719(1) Gauss) will be used. The resultant center frequency is

$$\upsilon_0(t) = 6834682624.(0) \text{ Hz}$$

The difference between this value and the frequency measured is 3470.8 Hz. The primary factors related to this center frequency shift are related to both rubidium clock lamp and the absorption cell temperatures (6:507). Since the measurement system used did not monitor these data points through the experiment, a comparison of these results to theoretical models could not be made. Applying the known magnetic field to Equation 2-34 does not provide any useful information. Center frequency shifts associated with low magnetic fields (100 to 200 mill-Gauss) are on the order of 200 to 300 Hz. However, even though the center frequency may be shifted, the primary Zeeman frequency relationship is very stable and is not affected by the same environmental changes. The magnetic field value determined from the Zeeman frequencies are commonly used today in highly accurate space magnetic field experiments.

Magnetic Field Model

The approach in evaluating the Helmholtz model also uses Equation 2-38. As discussed in the last section, accurate absorption cell current and Zeeman frequency measurements were obtained through the experiment. Applying the current values (I) measured to Equation 2-39 would result in a value for the magnetic field ($B_0(m)$). Substituting this value and the corresponding measured Zeeman frequency into Equation 2-38, would result in a determination of the constant term Kz(m). This value can then be compared to the theoretical Zeeman frequency constant, Kz(a). However, as seen in Figure 2.17 (page 2.37), there is no constant value obtained in using the Helmholtz model. As would be expected, the magnetic field is weaker near the ends of the absorption cell and strongest in the center. A least squares fit was applied to each curve associated with Figure 2.17, so that a constant value of B_0 could be used for each Zeeman frequency measured. Dividing the measured Zeeman frequency by this constant (B_0) value will determine Kz(m). Zeeman frequency measurements were obtained from current values varying from 3 to 20 milli-amps. The results of this comparison can be seen in Figure 4.1.

The results seem to indicate a fairly large difference (~16274 Hz/Gauss) between the two Kz terms. However, the error associated with the current measurement will propagate through the equations into an error associated with the value of Kz. The accuracy of the current measurement system used is $\pm$ 0.005 milli-amps. Translating this accuracy into the calculations which made up Kz(m) provides an error bound of $\pm$16967 Hz/Gauss. Therefore, the measured results, including the error, provide confidence that Kz(m) is within acceptable limits of the theoretical value. This error bound was also determined for the

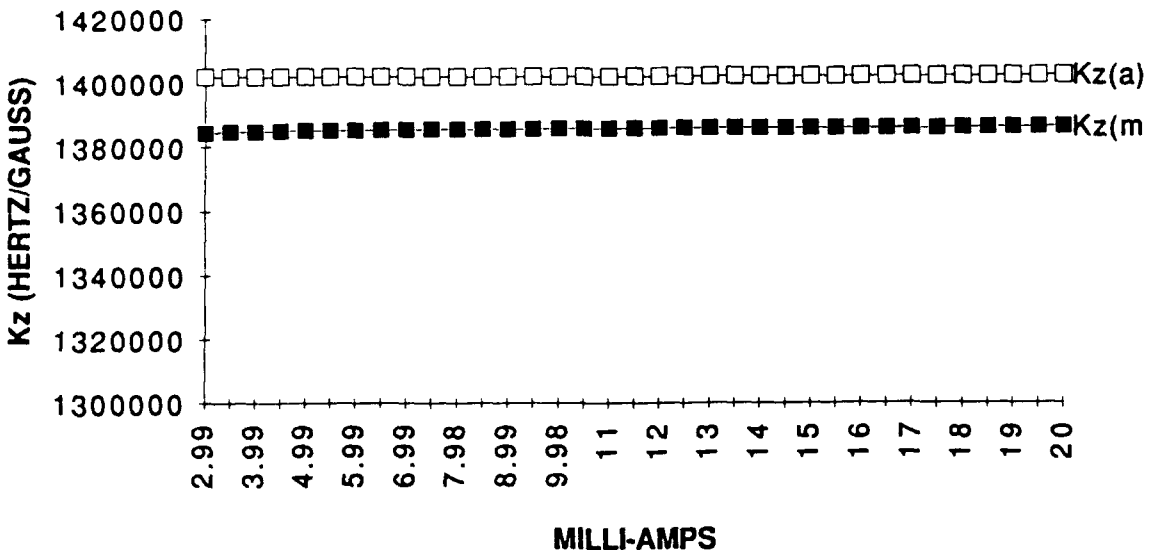

Figure 4.1 Measured Versus Theoretical Comparison of Zeeman Frequency Constant (Kz)

accuracy of the measured B_0 term and calculated as $\pm$ 0.15 milli-Gaus. This accuracy is sufficient when dealing with magnetic field values in the hundreds of milli-gauss, but not sufficient to evaluate the subtle effects of the measured hyperfine states at very low (<10 milli-gauss) ranges.

As shown in Figure 3.5, there exists two magnetic field values (9 and 27 milli-Gauss ($\pm$ 0.15), which resulted in minimizing output frequency shifts. This led to investigating the effects on the Zeeman frequencies at these low magnetic field ranges to identify potential reasons for this to occur. The magnetic field values where the zero crossings occur relate to current settings in the range of 0.2 to 0.9 milli-amps.

To investigate this area, the same approach as before was taken to determine the Zeeman constant Kz(m), except at lower coil current values (0 to 3 milli-amps). Figure 4.2 represents the results of calculating Kz(m) at these lower current values. A .01 milli-amp increment was used to plot the data.

The Kz(a) value is not plotted on this chart since the scale would distort the data by compressing the y axis scale, and masking some of the non-linear data..

These results seem to indicate indicate that there is a non-linear relationship between the Zeeman frequency and the resonance center frequency at both large magnetic fields (>1000 Gauss), and very small magnetic fields (<100 milli-Gauss). Theoretically, the Zeeman frequency determination is expected to be linear, but by some effect of the cell temperature or light temperature, a new component is factored into the magnetic field relationship.

A mathematical fit was applied to this non-linear region which provided fairly accurate results as compared to the measured data. The error per data point as well as average error for all the points are provided in Table 4.1. The largest error to the fit existed at the current value of 0.1 milli-amps. In addition, since there is a $\pm$ 0.005 milli-amp uncertainty in the measured value, there will be a small additional error in the difference calculation. As can be seen in Table 4.1, the measured data matches the mathematical curve well within 1%. If the same results could be obtained from other frequency sources at these low magnetic field settings, it could possibly validate this non-linear fit. This fit is represented by the following equation:

$$Kz = Ao\ e^{-(c/c+m)} \qquad 4.1$$

where

Ao = 1385000

c=.0037

m= current (milli-amps)

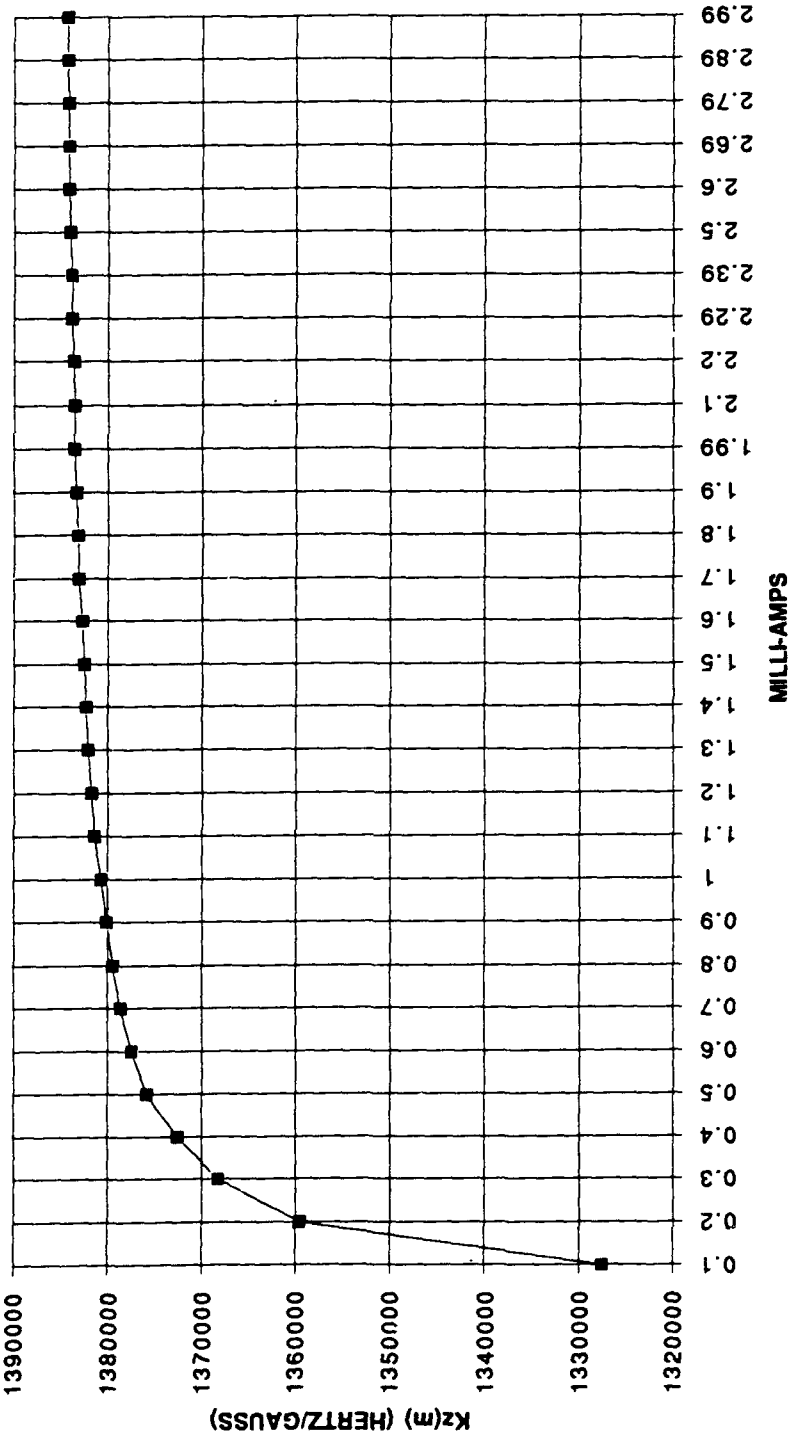

Figure 4.2 Measured Zeeman Frequency Constant Kz at Low Current Values

This would indicate that for practical clock operations the calculation for the Zeeman frequency would be represented by:

$$\upsilon_z = Ao\, e^{-[c/(c+m)]}\, Kz\, B_o \qquad 4.2$$

Since this is based on only one clock sample, it would be premature to incorporate this finding for all rubidium clocks. Further experiments on a greater sample of clocks may validate these results.

Table 4.1 Comparison of Zeeman Frequency Model to Measured Values

Current(ma)	e(-c/(c+m))	Kz	Kz(m)	(Kz(m)-Kz)/Kz(m)
0.1	0.9654	1,337,076	1,327,568	-0.72%
0.2	0.9822	1,360,398	1,359,550	-0.06%
0.3	0.9881	1,368,451	1,368,244	-0.02%
0.4	0.9910	1,372,533	1,372,592	0.00%
0.5	0.9928	1,374,999	1,375,853	0.06%
0.6	0.9940	1,376,651	1,377,843	0.09%
0.7	0.9948	1,377,834	1,378,647	0.06%
0.8	0.9955	1,378,724	1,379,520	0.06%
0.9	0.9960	1,379,417	1,380,199	0.06%
1	0.9964	1,379,972	1,380,734	0.06%
1.1	0.9967	1,380,427	1,381,484	0.08%
1.2	0.9970	1,380,806	1,381,830	0.07%
1.3	0.9972	1,381,128	1,382,122	0.07%
1.4	0.9974	1,381,403	1,382,373	0.07%
1.5	0.9976	1,381,642	1,382,590	0.07%
1.6	0.9977	1,381,851	1,382,781	0.07%
	AVERAGE of	MAGNITUDE of	DIFFERENCES =	0.00%

Resonance and Zeeman Frequency

My original hypothesis at the beginning of this study was that there should be a correlation of Zeeman frequency changes with fractional frequency differences. However, this was not the case. The Zeeman frequencies were exactly the same for all the power variations, at the same magnetic field settings. The exception to this rule was discussed in the previous section. Analyzing the Zeeman frequency data at coil currents from 1 to 20 milli-amps reflected changes in the range of 0.04 Hz. Since this is an area of uncertainty in frequency measurement, these results were not considered valid.

The other area to investigate was any apparent relationship between the center frequency and fractional frequency as a function of the coil magnetic field. Equation 2.34 indicates that there is a proportional difference in center frequency to the square of B_0. *Figure 4.3 represents a plot of the center* frequency as a function of magnetic field from 0 to 0.6 Gauss. Figure 4.4 represents a plot of the measured fractional frequency data is represented in terms of magnetic field, at a constant microwave power (P_0). The measured current values were converted to magnetic field values for purposes of comparing the two figures. The error associated with the magnetic field, as determined earlier, is negligible on the scale presented in Figure 4.4. A curve fit was applied to Figure 4.4 using current (I) as the variable:

$$[\Delta f / f_0] \, (10^{-9}) = -1.6169 + .013027 \, (I) + .075969 \, (I)^2 \qquad 4.2$$

where

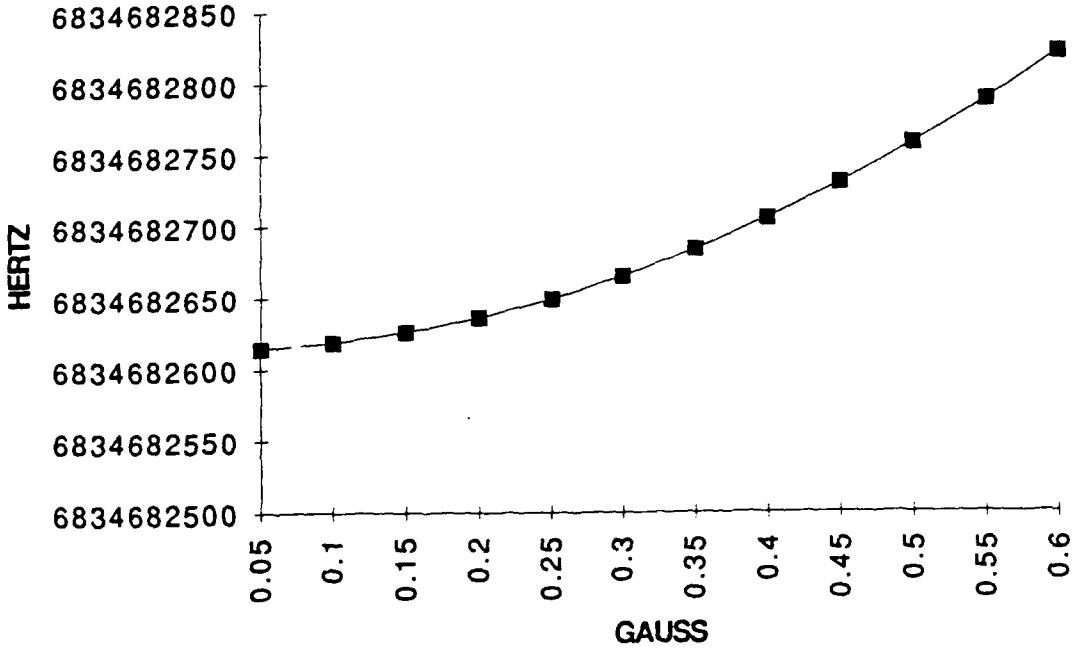

Figure 4.3 Center Frequency (Theoretical) Change as a Function of B_o

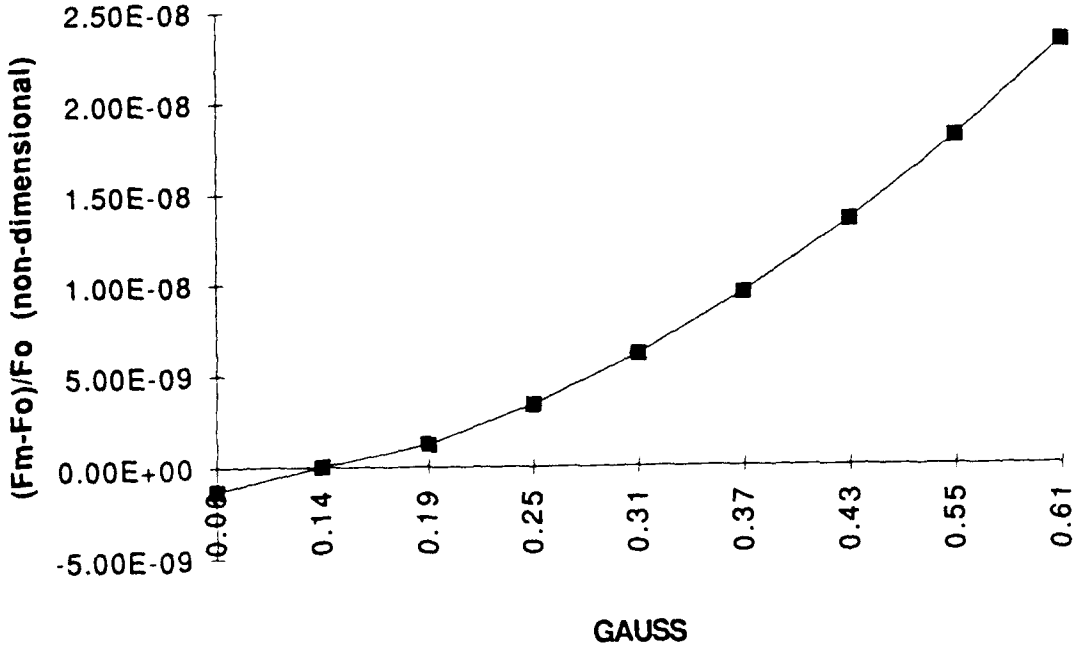

Figure 4.4 Fractional Frequency as a Function of B_o

f_0 = 10 Mhz reference output frequency

I = current in milli-amps

No correlation was established between the expected center frequency shift and the error observed in the measurements.

Resonance Half Power Linewidth

The differences in frequency of the half power linewidth and center frequencies were provided in Table 3.1. The measurements were taken relative to the nominal factory microwave power setting, P_0. The half-power measurement is 1/2 the change in resonance output signal voltage measured in milli-volts (mV).

Figure 3.9 indicates the obvious decay in signal output voltage as a function of decreasing cavity microwave power. As the power was decreased, it was evident through observing the plots that the power broadening effect made finding the center frequency value very difficult. This can be seen in Figure 4.5, which represents the center frequency plot at a point 4dB below the nominal setting. Since internal frequency adjustments are made through lamp intensity changes to keep the quartz crystal on the rubidium center frequency, it is quite evident through the plot that the light sensor would need to be quite sensitive. The frequency shift at these power settings were the largest, which is what one would expect.

As the power is increased toward P_0 the resonance lines become sharper, and easier to determine the center frequency. This data substantiates the fractional frequency results presented in Figure 3.4.

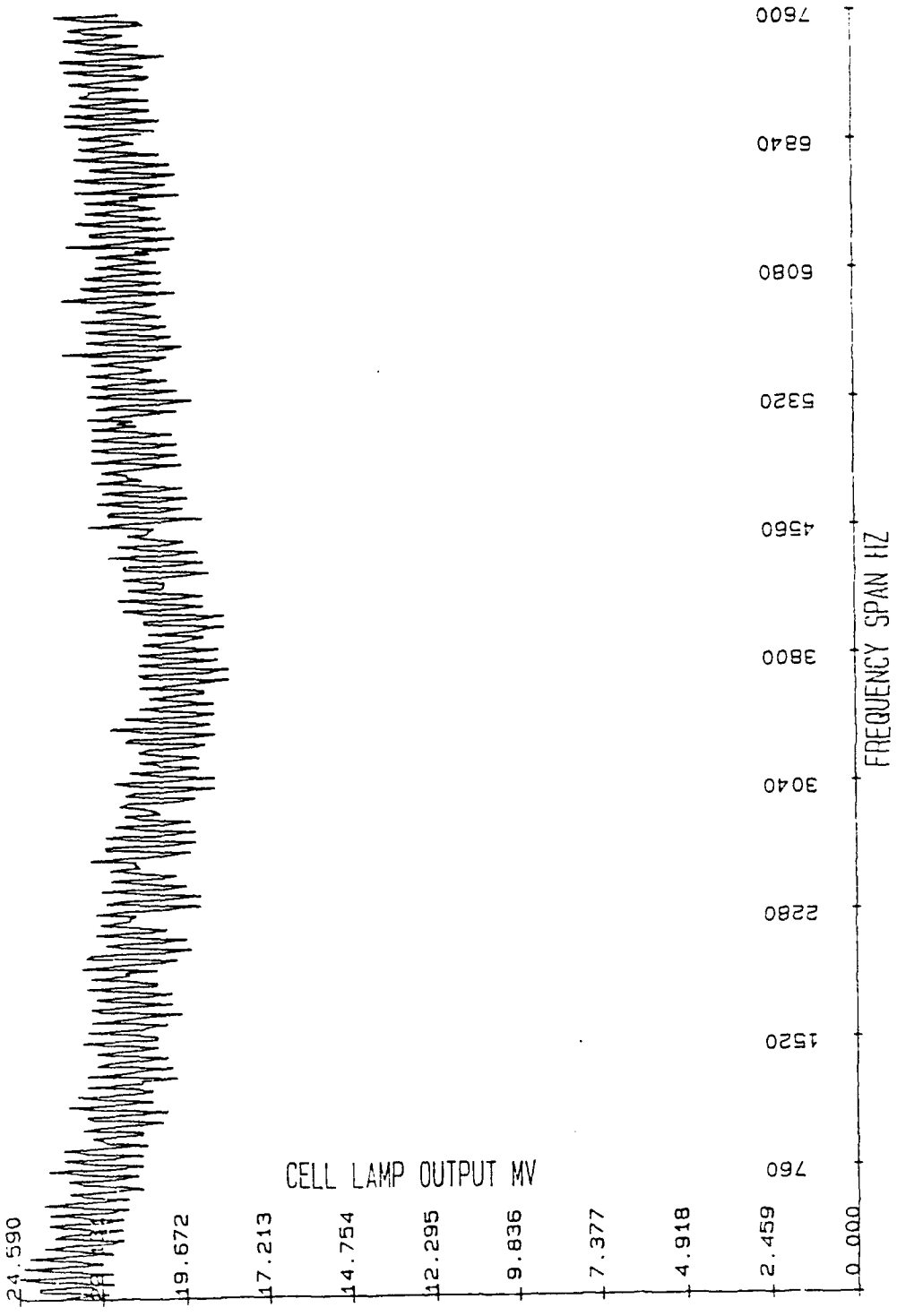

Figure 4.5 Center Frequency (υ_0) Line Width Plot for RFS-10 Rubidium Clock at 4dB Below Nominal Factory Power Setting

In summary, the maximum frequency change observed for the +1.3 and -1.1 dB data is about 3×10^{-11}, for the -2.2 dB data is about 6×10^{-11}, and that for the -4.0 dB data is about 1.4×10^{-10}. As a function of the change in microwave power, the maximum frequency change is about 2.6×10^{-11}/dB. The curves represented in Figure 3.4 have a similar shape, namely one that is fairly flat for Zeeman frequencies between 100 and 300 kHz, then decreasing for Zeeman frequencies between 300 and 850 kHz.

There was also evidence of zero crossings at Zeeman frequencies of about 13 and 37 kHz. The operation of this clock at one of these points resulted in zero sensitivity of the clock frequency to microwave power changes.

The manufacturer's B-field current setting for this clock was 4.5 milli-amps, which gave a Zeeman frequency of about 191 kHz. Operating the clock at lower B-fields would also have the advantage of decreasing clock sensitivity to B-field current; i.e., a change in B-field current results in a smaller change in output frequency when the B-field current is small.

The maximum frequency change due to microwave power variations was about 2.6×10^{-11} per dB of power change. At this B-field setting an Allan standard deviation of 0.01 dB in the microwave power would result in an Allan standard deviation in the frequency of 2.6×10^{-13} from the power changes alone.

V *Conclusions and Recommendations*

The experimental results I have presented here regarding the interaction of the B-field and the microwave power on the output frequency were conducted on only one commercial rubidium clock. The results have shown that, in this particular case, this clock is very sensitive to microwave power variations or fluctuations.

Adjustment of the coil magnetic field to the values observed in this experiment to minimize output frequency changes is not recommended at this time. Further tests need to be conducted on a variety of clocks to validate this data.

The zero crossings that were observed, however, may be interpreted in terms of (1) the opposing effect of the spatially inhomogeneous light shift and (2) the C-field gradient; the light shift produces a positive frequency shift, while the C-field gradient produces a negative frequency shift (6:506-513). A different test configuration would be required to validate this interpretation. I recommend that these light shift effects be investigated experimentally using the same frequency clock. Correlation of data provided here with those results could provide more insight into rubidium accuracy and stability for space and commercial applications.

APPENDIX A

CALCULATION OF FREQUENCY STABILITY

Frequency stability in the time domain is expressed as the two-sample (Allan) variance, $\sigma_y^2(t)$.

$$\sigma_y^2(t) = 1/2[y_{k+1} - y_k)^2$$

where the brackets denotes an average over a number of data points and y_k is the average fractional frequency over time of the data point k.

Stability of a frequency standard typically exhibits the characteristics of the figure below.

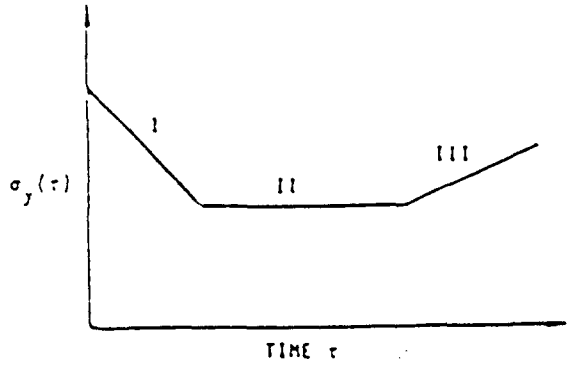

Typical Stability Characteristics

The first part, "I", reflects the fundamental noise properties of the standard. This decreasing behavior continues with increasing averaging time until the "flicker floor" is reached, II, where the frequency stability σ_y is independent of

the averaging time. The third part of the curve, III, represents the stability deterioration with increasing averaging time. This typically occurs at times ranging from minutes to days, depending on the standard.

BIBLIOGRAPHY

1. Allan, David W. Synchronization of Clocks, Keynote Address. Frequency Symposium, Pasedena, Ca., 1991.

2. Audin, Claude and Jacques Vanier. The Quantum Physics of Atomic Frequency Standards, Volumn 1. Bristol, England: 10P Publishing Ltd., 1989.

3. Audin, C. et al. Physical Origin of the Frequency Shifts in Cesium Beam Frequency Standards: Related Environmental Sensitivity. 419-440. 41st Frequency Control Symposium, 419-440. Philadelphia Pa., 1987.

4. Beyer, William, H. CRC Standard Mathematical Tables. Boca Raton, Fl.: CRC Preess, Inc., 1979.

5. Bloom, Arnold L. Optical Pumping. Proceeds of the 4th European Frequency and Time Forum. 72-80. Neuchatel, March 1990.

6. Busca, G. and Risley, A. Effect of Line Inhomogeneity on the Frequency of Passive Rb 87 Frequency Standards. Proceedins of the Symposium in Frequency Standards. 506-513 Boulder Co., 1978.

7. Campero, J.C. et al. Inhomogeneous Light Shift in Alkali-Metal Atoms. Physical Review A, Volumn 27, Number 4. *Los Angeles:* The American Physical Society, 1983.

8. Candler, Chris. Atomic Spectra and the Vector Model. Princeton, Pa.: D. Van Nostrend Company, Inc., 1964.

9. Carver, Thomas R. Optical Pumping, Science, Volume 141, Number 3581. 599-607. 16 August 1963.

10. Condon, E.U. Handbook of Physics. New York: McGraw-Hill, Inc. 1967.

11. DiMarchi, Andrea. Improving the Long Term Stability of Cesium Beam Frequency Standards. Proceed of 4th European Frequency and Time Forum. 517-521. Neuchatel, March 1990.

12. DiMarchi, Andrea. New Insights Into Causes and Cures of Frequency Instabilities(Drift and Long Term Noise) In Cesium Beam Frequency Standards. 41st Frequency Control Symposium, 54-58. Philadelphia Pa., 1987.

13. Eisberg, Robert M. Fundamentals of Modern Physics. New York: John Wiley & Sons, Inc., 1967.

14. Frequency Standards and Clocks. Application Note 101. Frequency and Time Systems, Inc., Beverly, Ma, 1983.

15. Halliday, David and Resrick, Robert. Fundamentals of Physics.
New York: John Wiley & Sons, Inc., 1970.

16. Hayt, William H. Jr. Engineering Electromagnetics.
New York: McGraw-Hill, Inc., 1989.

17. Hellwig, Helmut. Oscillator Instabilities and Frequency Changes. Internal NBS Report. National Bureau of Standards, Boulder, Co., 1979.

18. Kartaschoff, P. Frequency and Time.
New York: Academic Press, 1978.

19. Model RFS-10 Rubidium Frequency Standard. Technical Information. Salem, Ma: EG&G Frequency Products, Feb 1985.

20. Ramsey, Norman, F. Molecular Beams
Oxford: Clarendon Press. 1956.

22. Semler, James R. Common-View GPS Time Transfer Accuracy and Stability Results. 41st Frequency Control Symposium, 537-548. Philadelphia Pa., 1987.

23. Time and Frequency Measurements, Application Note 102, Frequency and Time Systems, Inc., Beverly, Ma, 1983.

24. U.S. Department of Commerce. The Measurement of Frequency and Frequency Stability. National Bureau of Standards Technical Note 669. Washington: Government Printing Office, 1975.

25. Weidner, Richard T. in collaboration with Michael E. Brown.
Physics, Part Two. Boston: Allyn and Bacon, Inc., 1985.

Vita

Major Edward B. Sarosy was born on 3 July 1954 in Painesville, Ohio. He graduated from St. Joseph High School in Cleveland, Ohio in 1972 and attended the University of Miami, graduating with a Bachelor of Science in Electrical Engineering in May 1976. Upon graduation, he received a reserve commission in the USAF from AFROTC as a distinguished graduate. He served his first tour at Vandenberg AFB, CA in the 10th Aerospace Defense Squadron within the Air Defense Command. He began as an Electronics Test Enginner where he directed all pre-launch activities on the Thor booster for the Defense Meteorological Satellite Program. He was then selected to manage the enegineering analysis branch for the Air Launched Anti-Satellite Test Program in January 1982 within the 6595th Aerospace Test Group. He was then chosen to work classified space-related acquisition program for Space Systems Division at Los Angeles AFB, CA. There he was the program manager for a multi-million dollar special access required space defense system.

REPORT DOCUMENTATION PAGE

Form Approved
OMB No 0704-0188

1. AGENCY USE ONLY (Leave blank)	2. REPORT DATE	3. REPORT TYPE AND DATES COVERED
	September 1992	Final Thesis

4. TITLE AND SUBTITLE
OUTPUT FREQUENCY CHANGES IN A COMMERCIAL RUBIDIUM CLOCK RESULTING FROM MAGNETIC FIELD AND MICROWAVE POWER VARIATIONS

5. FUNDING NUMBERS
N/A

6. AUTHOR(S)

7. PERFORMING ORGANIZATION NAME(S) AND ADDRESS(ES)
Air Force Institute of Technology
Wright Patterson AFB, OH

8. PERFORMING ORGANIZATION REPORT NUMBER
N/A

9. SPONSORING/MONITORING AGENCY NAME(S) AND ADDRESS(ES)
N/A

10. SPONSORING/MONITORING AGENCY REPORT NUMBER
N/A

11. SUPPLEMENTARY NOTES

12a. DISTRIBUTION/AVAILABILITY STATEMENT
Approved for Public Release, Distribution Unlimited

12b. DISTRIBUTION CODE

13. ABSTRACT (Maximum 200 words)

This report shows the relationship between output frequency shifts and the absorption cell magnetic field during microwave power flunctuations on a commercial rubidium frequency clock. Changes in the clock output frequency relative to the 10 MHz reference were monitored as changes in the absorption cell magnetic field (0.01 to 1.0 Gauss) and changes in the cell's interrogation microwave power were varied from the nominal specification (P_o) at four discrete values (+1.3, -1.1, -2.2, -4.0dB). The maximum normalized output frequency shift of 1.4×10^{-10} occurred at -4dB. The maximum normalized frequency change for the +1.3 and -1.1 dB data is about 3×10^{-11}, and for the -2.2 dB data is about 6×10^{-11}. As a function of the change in microwave power, the maximum frequency change is about 2.6×10^{-11} per dB of power change. There also existed several magnetic field values which resulted in minimum output frequency change. This occurred at absorption cell magnetic field values of 9 and 27 milli-Gauss, where the nominal setting is 137 milli-Gauss.

14. SUBJECT TERMS
RUBIDIUM HYPERFINE ENERGY LEVELS

15. NUMBER OF PAGES
100

16. PRICE CODE

17. SECURITY CLASSIFICATION OF REPORT	18. SECURITY CLASSIFICATION OF THIS PAGE	19. SECURITY CLASSIFICATION OF ABSTRACT	20. LIMITATION OF ABSTRACT
UNCLASSIFIED	UNCLASSIFIED	UNCLASSIFIED	UL